Supporting Information

Photophysical, photostability, and *ROS* generation properties of new trifluoromethylated quinoline-phenol Schiff bases

Inaiá O. Rocha[1], Yuri G. Kappenberg[1], Wilian C. Rosa[1], Clarissa P. Frizzo[1], Nilo Zanatta1, Marcos A. P. Martins[1], Isadora Tisoco[2], Bernardo A. Iglesias[2] and Helio G. Bonacorso[1,*]

Address:

[1]Núcleo de Química de Heterociclos (NUQUIMHE), Departamento de Química, Universidade Federal de Santa Maria, Santa Maria, RS, 97105-900, Brazil

[2]Laboratório de Bioinorgânica e Materiais Porfirínicos, Departamento de Química, Universidade Federal de Santa Maria, Santa Maria, RS, 97105-900, Brazil

Email:

Helio Gauze Bonacorso - helio.bonacorso@ufsm.br

1. Crystallographic Data

Single crystals of compound **3ba** were obtained by slow evaporation of $CDCl_3$ at 25 °C. Diffraction measurement of compound **3ba** was performed using a Bruker D8 QUEST diffractometer using Cu Kα radiation (λ = 1.54178 Å) with a KAPPA four-circle goniometer equipped with a PHOTON II CPAD area detector, at a temperature of 296 K. Absorption corrections were performed using semi-empirical from equivalents methods. Non-hydrogen atoms were refined using anisotropic displacement parameters. The positions of the hydrogen atoms were calculated for idealized positions. The structure was solved and refined using the WinGX software package. [1] The structures were refined based on the full-matrix least-squares method using the SHELXL program. [2] The ORTEP projections of the molecular structures were generated using the ORTEP-3 program. [1] Crystallographic information file (CIF) for the novel structure was deposited at the Cambridge Crystallographic Data Centre (CCDC) under identification number 2036933 (**3ba**). Crystallographic data can be observed in the supporting information (Figure S1 and Table S1-S2).

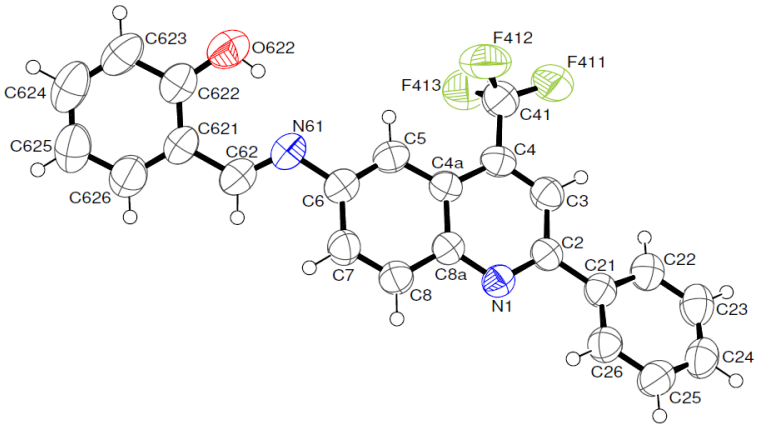

Figure S1. ORTEP of the Schiff base (**3ba**) (CCDC 2036933).

checkCIF/PLATON report

You have not supplied any structure factors. As a result the full set of tests cannot be run.

THIS REPORT IS FOR GUIDANCE ONLY. IF USED AS PART OF A REVIEW PROCEDURE FOR PUBLICATION, IT SHOULD NOT REPLACE THE EXPERTISE OF AN EXPERIENCED CRYSTALLOGRAPHIC REFEREE.

No syntax errors found. CIF dictionary Interpreting this report

Datablock: shelx

```
Bond precision:  C-C = 0.0045 A          Wavelength=1.54178

Cell:            a=4.9442(2)     b=25.5275(12)      c=14.6982(7)
                 alpha=90        beta=98.687(3)     gamma=90
Temperature:     296 K

                 Calculated                Reported
Volume           1833.82(14)               1833.82(14)
Space group      P 21/c                    P 21/c
Hall group       -P 2ybc                   -P 2ybc
Moiety formula   C23 H15 F3 N2 O           C23 H14 N2 O1 F3
Sum formula      C23 H15 F3 N2 O           C23 H15 F3 N2 O
Mr               392.37                    392.37
Dx,g cm-3        1.421                     1.421
Z                4                         4
Mu (mm-1)        0.921                     0.921
F000             808.0                     808.0
F000'            810.85
h,k,lmax         5,30,17                   5,30,17
Nref             3348                      3154
Tmin,Tmax        0.898,0.946               0.635,0.753
Tmin'            0.773

Correction method= # Reported T Limits: Tmin=0.635 Tmax=0.753
AbsCorr = MULTI-SCAN

Data completeness= 0.942          Theta(max)= 68.384

R(reflections)= 0.0563( 1592)     wR2(reflections)= 0.1512( 3154)

S = 1.012                 Npar= 262
```

The following ALERTS were generated. Each ALERT has the format
test-name_ALERT_alert-type_alert-level.
Click on the hyperlinks for more details of the test.

Table S1. Crystal data and structure refinement for compound **3ba**

Compound	**3ba**
CCDC number	2036933
Empirical formula	$C_{23}H_{15}F_3N_2O$
Molecular weight	392.37
Temperature (K)	296(2)
Wavelength (Å)	1.54178
Crystal system	Monoclinic
Space group	$P2_1/c$
Cell parameters	
a (Å)	4.9442(2)
b (Å)	25.5275(12)
c (Å)	14.6982(7)
α (°)	90
β (°)	98.687(3)
γ (°)	90
Volume (Å^3)	1833.82(14)
Z	4
Calculated density (Mg/m^3)	1.421
Abs. coef. (mm^{-1})	0.921
F (000)	808
Crystal size (mm)	0.279 x 0.097 x 0.060
θ range for data collection (°)	3.500 to 68.384
h, k, l range	-5<=h<=5, -30<=k<=30, -17<=l<=17
Reflections collected / unique	11117 / 3154 [R(int) = 0.0685]

Completeness to theta (%)	94.2
Absorption correction	Semi-empirical from equivalents
Max. and min. transmission	0.7531 and 0.6354
Refinement method	Full-matrix least-squares on F^2
Data / restraints / parameters	3154 / 0 / 262
Goodness-of-fit on F^2	1.012
Final R indices	R1 = 0.0563, wR2 = 0.1175
R all data	R1 = 0.1375, wR2 = 0.1512
Extinction coefficient	None
$\Delta \rho_{máx.}$ and $\Delta \rho_{min}$ (e A^{-3})	0.149 and -0.169

Table S2. Bond lengths [A] and angles [°] for compound **3ba**

F(412)-C(41)	1.337(4)	C(622)-C(621)-C(62)	121.7(3)
F(413)-C(41)	1.329(4)	N(61)-C(62)-C(621)	123.5(3)
F(411)-C(41)	1.323(4)	N(61)-C(62)-H(62)	118.2
O(622)-C(622)	1.351(4)	C(621)-C(62)-H(62)	118.2
O(622)-H(622)	0.8200	C(5)-C(6)-C(7)	120.3(3)
N(61)-C(62)	1.272(4)	C(5)-C(6)-N(61)	116.7(3)
N(61)-C(6)	1.427(4)	C(7)-C(6)-N(61)	123.1(3)
N(1)-C(2)	1.318(3)	C(6)-C(5)-C(4A)	121.3(3)
N(1)-C(8A)	1.364(3)	C(6)-C(5)-H(5)	119.4
C(624)-C(623)	1.362(5)	C(4A)-C(5)-H(5)	119.4
C(624)-C(625)	1.373(5)	C(4)-C(4A)-C(5)	126.3(3)
C(624)-H(624)	0.9300	C(4)-C(4A)-C(8A)	115.5(3)
C(625)-C(626)	1.380(5)	C(5)-C(4A)-C(8A)	118.2(3)

C(625)-H(625)	0.9300	C(3)-C(4)-C(4A)	120.2(3)
C(626)-C(621)	1.383(4)	C(3)-C(4)-C(41)	119.0(3)
C(626)-H(626)	0.9300	C(4A)-C(4)-C(41)	120.8(3)
C(621)-C(622)	1.386(4)	C(4)-C(3)-C(2)	120.5(3)
C(621)-C(62)	1.453(4)	C(4)-C(3)-H(3)	119.7
C(62)-H(62)	0.9300	C(2)-C(3)-H(3)	119.7
C(6)-C(5)	1.359(4)	N(1)-C(2)-C(3)	121.5(3)
C(6)-C(7)	1.408(4)	N(1)-C(2)-C(21)	117.1(3)
C(5)-C(4A)	1.423(4)	C(3)-C(2)-C(21)	121.3(3)
C(5)-H(5)	0.9300	C(26)-C(21)-C(22)	118.1(3)
C(4A)-C(4)	1.412(4)	C(26)-C(21)-C(2)	119.9(3)
C(4A)-C(8A)	1.427(4)	C(22)-C(21)-C(2)	122.0(3)
C(4)-C(3)	1.358(4)	C(23)-C(22)-C(21)	121.1(3)
C(4)-C(41)	1.495(4)	C(23)-C(22)-H(22)	119.4
C(3)-C(2)	1.414(4)	C(21)-C(22)-H(22)	119.4
C(3)-H(3)	0.9300	C(24)-C(23)-C(22)	120.2(3)
C(2)-C(21)	1.481(4)	C(24)-C(23)-H(23)	119.9
C(21)-C(26)	1.387(4)	C(22)-C(23)-H(23)	119.9
C(21)-C(22)	1.389(4)	C(23)-C(24)-C(25)	119.7(3)
C(22)-C(23)	1.378(4)	C(23)-C(24)-H(24)	120.2
C(22)-H(22)	0.9300	C(25)-C(24)-H(24)	120.2
C(23)-C(24)	1.366(4)	F(411)-C(41)-F(413)	106.4(3)
C(23)-H(23)	0.9300	F(411)-C(41)-F(412)	105.6(3)
C(24)-C(25)	1.372(4)	F(413)-C(41)-F(412)	106.2(3)
C(24)-H(24)	0.9300	F(411)-C(41)-C(4)	113.1(3)

C(25)-C(26)	1.383(4)	F(413)-C(41)-C(4)	112.4(3)
C(25)-H(25)	0.9300	F(412)-C(41)-C(4)	112.5(3)
C(26)-H(26)	0.9300	C(24)-C(25)-C(26)	120.7(3)
C(8A)-C(8)	1.410(4)	C(24)-C(25)-H(25)	119.7
C(8)-C(7)	1.363(4)	C(26)-C(25)-H(25)	119.7
C(8)-H(8)	0.9300	C(25)-C(26)-C(21)	120.3(3)
C(7)-H(7)	0.9300	C(25)-C(26)-H(26)	119.9
C(622)-C(623)	1.396(4)	C(21)-C(26)-H(26)	119.9
C(623)-H(623)	0.9300	N(1)-C(8A)-C(8)	117.6(3)
C(622)-O(622)-H(622)	109.5	N(1)-C(8A)-C(4A)	123.6(3)
C(62)-N(61)-C(6)	119.9(3)	C(8)-C(8A)-C(4A)	118.8(3)
C(2)-N(1)-C(8A)	118.6(2)	C(7)-C(8)-C(8A)	121.3(3)
C(623)-C(624)-C(625)	121.2(4)	C(7)-C(8)-H(8)	119.4
C(623)-C(624)-H(624)	119.4	C(8A)-C(8)-H(8)	119.4
C(625)-C(624)-H(624)	119.4	C(8)-C(7)-C(6)	120.2(3)
C(624)-C(625)-C(626)	118.5(4)	C(8)-C(7)-H(7)	119.9
C(624)-C(625)-H(625)	120.8	C(6)-C(7)-H(7)	119.9
C(626)-C(625)-H(625)	120.8	O(622)-C(622)-C(621)	122.2(3)
C(625)-C(626)-C(621)	121.9(4)	O(622)-C(622)-C(623)	118.1(3)
C(625)-C(626)-H(626)	119.0	C(621)-C(622)-C(623)	119.7(3)
C(621)-C(626)-H(626)	119.0	C(624)-C(623)-C(622)	120.2(4)
C(626)-C(621)-C(622)	118.5(3)	C(624)-C(623)-H(623)	119.9
C(626)-C(621)-C(62)	119.8(3)	C(622)-C(623)-H(623)	119.9

2. Photophysical Analyses and Photostability Assays

For spectroscopic analysis, UV-Vis absorption spectra were recorded using a Shimadzu UV2600 spectrophotometer (2.0 nm data range), using DMSO, MeOH or chloroform as solvent. The steady-state emission fluorescence spectra in DMSO, MeOH or chloroform solutions were measured with a Cary50 Eclipse Fluorescence Spectrophotometer (excitation/emission; slit 2.5 mm). The values of the quantum fluorescence yield (Φ_f) were determined in solution, using the compound 9,10-diphenylanthracene (DPA) in chloroform (Φ_f = 0.65, λ_{exc} = 366 nm) as a comparison emission standard, according Equation (1):

$$\phi_f = \phi_f^{ref} \; x \; \frac{\int_{\lambda_0}^{\lambda_f} F(\lambda)\, d\lambda}{\int_{\lambda_0}^{\lambda_f} F_{ref}(\lambda)\, d\lambda} \; x \; \frac{f_{ref}}{f} \; x \; \frac{n^2}{n_{ref}^2} \quad \textbf{(1)}$$

in which ϕ_f^{ref} is the standard fluorescence quantum yield (Φ_f = 0.65, 9,10-Diphenylanthracene - DPA dissolved in $CHCl_3$), $F(\lambda)$´s are the fluorescence spectra (samples and reference) integrate in all emission range, n is the solvent refractive index and f is the quantity of light that is absorbed at the excitation wavelength, given by: $f = 1 - 10^{-A(\lambda_{ex})}$, in which A is the absorbance.

Photostability assays were performed using white-light LED array system irradiation (visible range) at 25 mW/cm^2 and total light dosage 90 J/cm^2 at 60 min, according to the current literature [3–5]. All experiments were performed in duplicate and independently.

DMSO solutions of compounds at 1.0 µM were freshly prepared and kept in the dark at room temperature. The photo-irradiation experiments were performed in magnetically stirred cuvette solutions (with 2.0 mL of sample), over a period of 30 min with white-light LED array system at fluence of 25 mW/cm^2 and total light dosages of 90 J/cm^2 (60 min). The absorbance was determined before irradiation and at 0, 5, 10, 15, 20, 30, 40, 50 and 60 min after irradiation. The results were expressed as follows using Equation (2):

$$Photostability(\%) = \frac{Abs\ at\ a\ given\ time\ of\ irradiation}{Abs\ before\ irradiation} x100\% \quad \textbf{(2)}$$

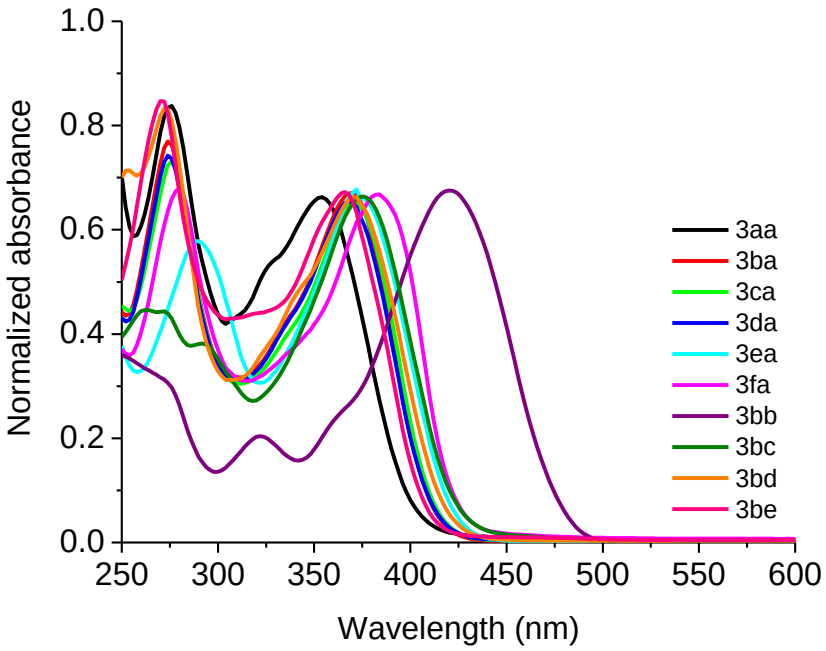

Figure S2. UV-Vis absorption spectra of compounds **3aa-fa** and **3bb-be** in $CHCl_3$ solution ([ ] = 1.50 x 10^{-5} M).

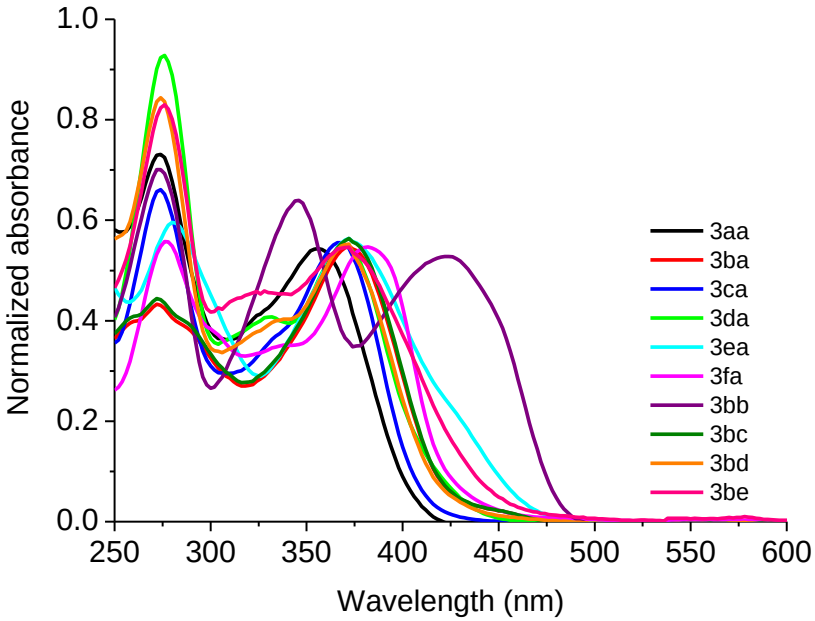

Figure S3. UV-Vis absorption spectra of compounds **3aa-fa** and **3bb-be** in MeOH solution ([ ] = 1.50 x 10^{-5} M).

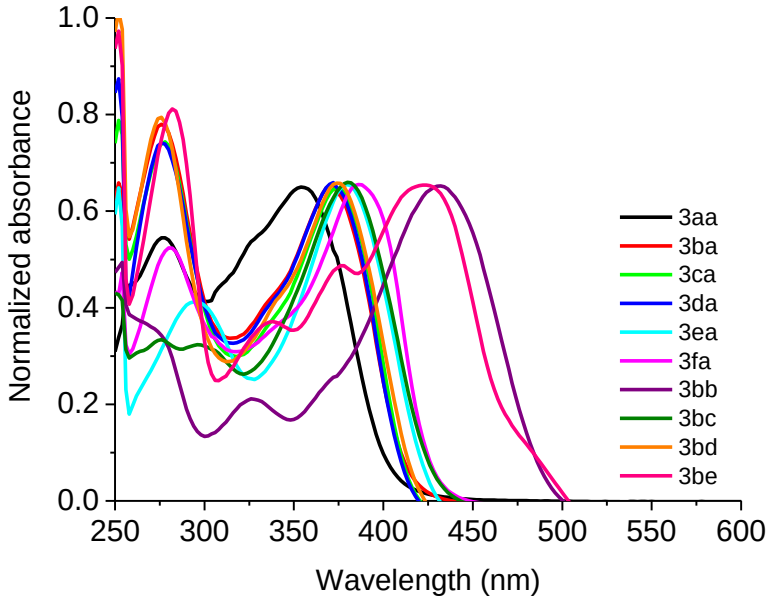

Figure S4. UV-Vis absorption spectra of compounds **3aa-fa** and **3bb-be** in DMSO solution ([ ] = 1.50 x 10^{-5} M).

(a)

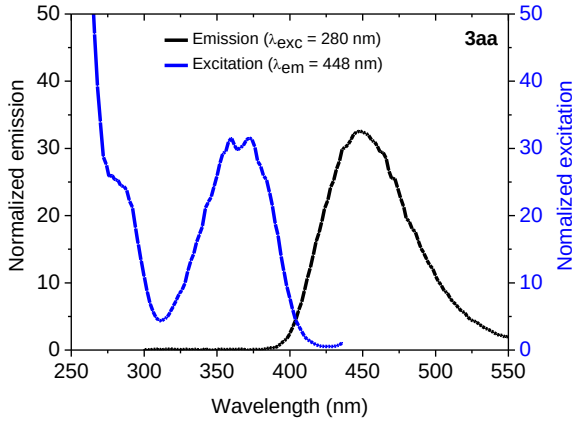

(b)

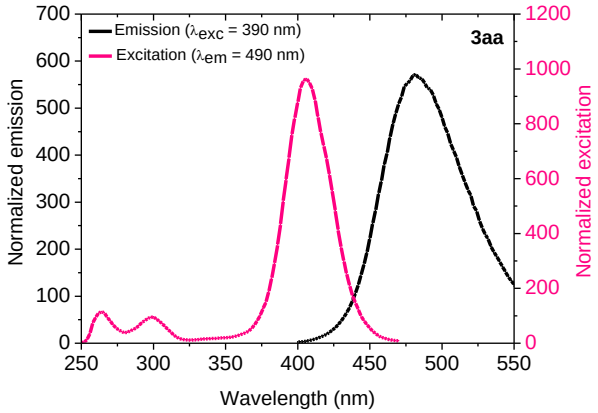

(c)

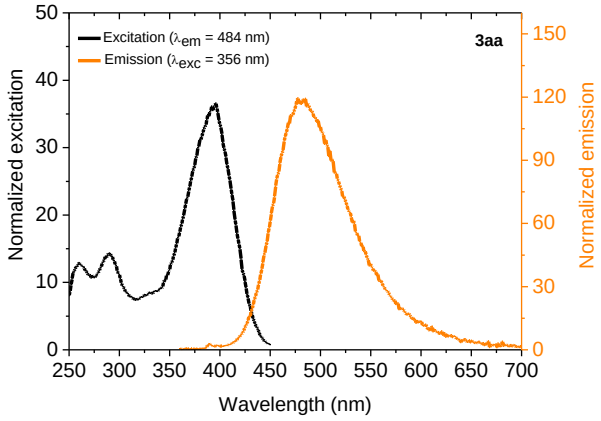

Figure S5. Steady-state emission fluorescence spectra of compound **3aa** in **(a)** $CHCl_3$, **(b)** DMSO and **(c)** MeOH ([ ] = 1.50 x 10^{-5} M).

(a)

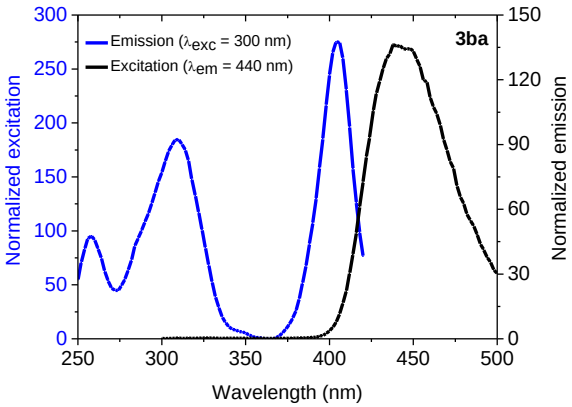

(b)

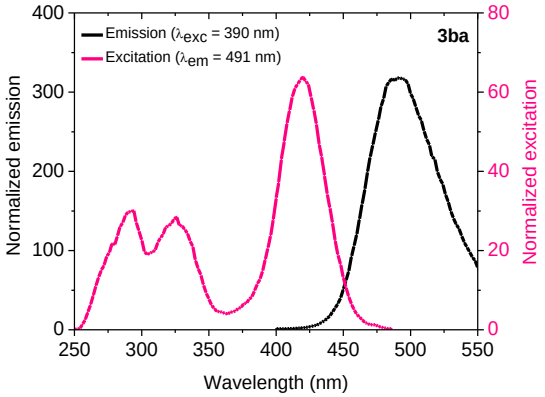

(c)

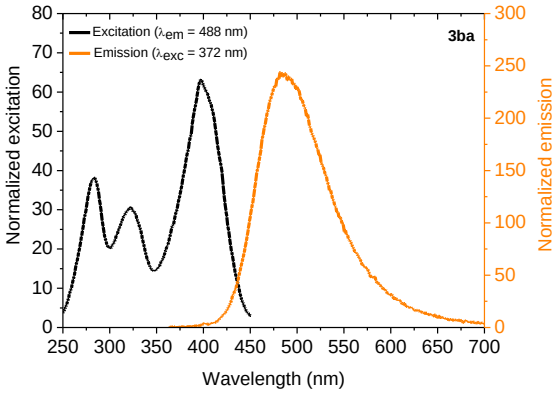

Figure S6. Steady-state emission fluorescence spectra of compound **3ba** in **(a)** $CHCl_3$, **(b)** DMSO and **(c)** MeOH ([ ] = 1.50 x 10^{-5} M).

(a)

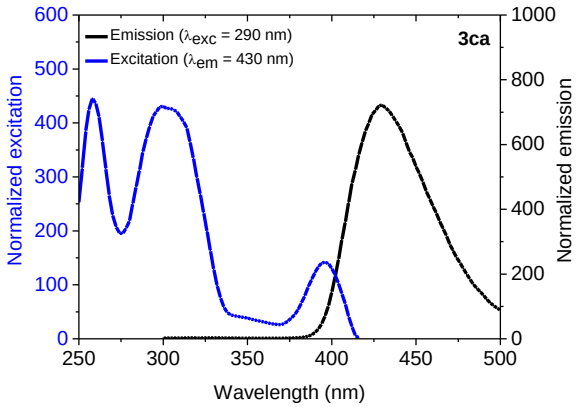

(b)

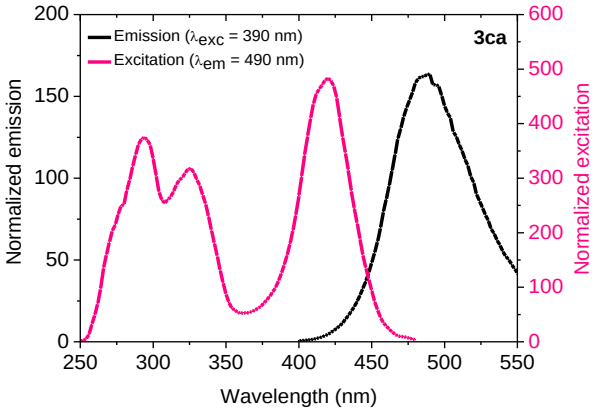

(c)

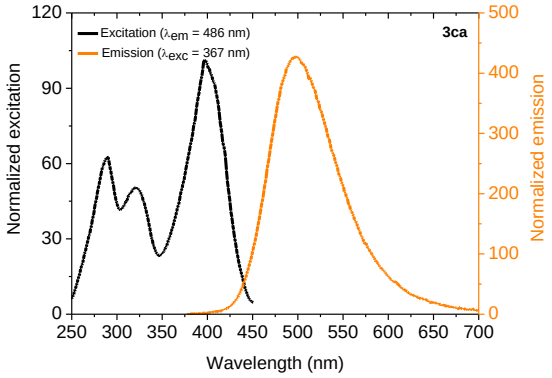

Figure S7. Steady-state emission fluorescence spectra of compound **3ca** in **(a)** $CHCl_3$, **(b)** DMSO and **(c)** MeOH ([ ] = 1.50 x 10^{-5} M).

(a)

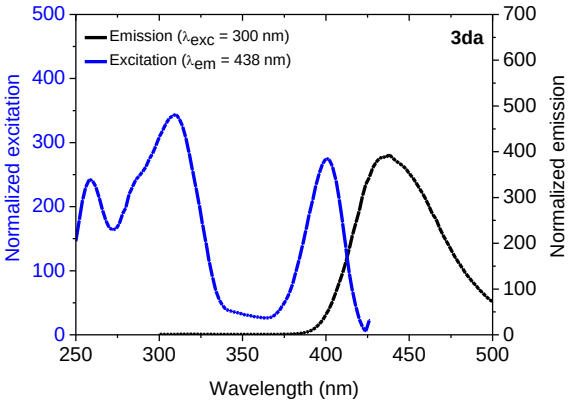

(b)

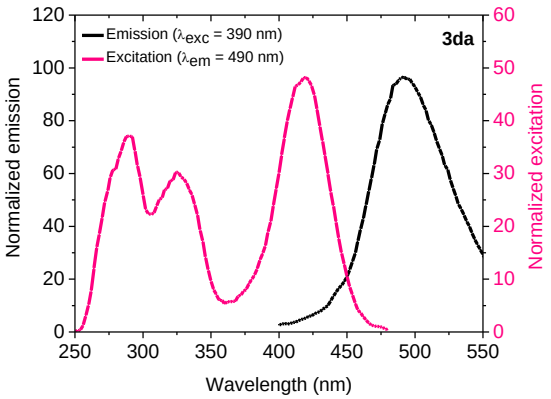

(c)

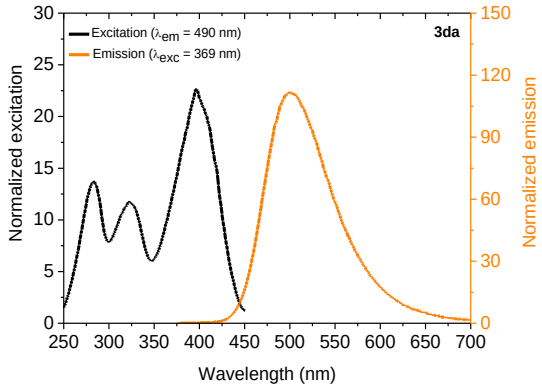

Figure S8. Steady-state emission fluorescence spectra of compound **3da** in **(a)** $CHCl_3$, **(b)** DMSO and **(c)** MeOH ([ ] = 1.50 x 10^{-5} M).

(a)

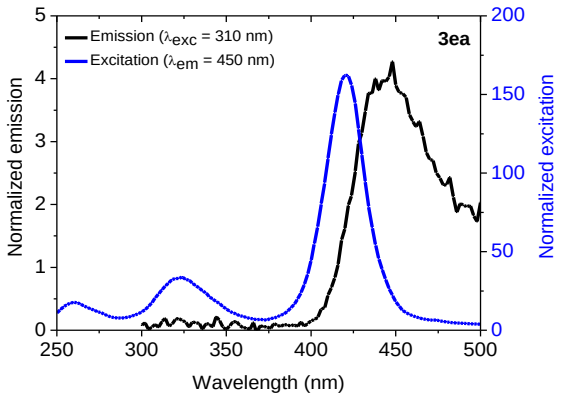

(b)

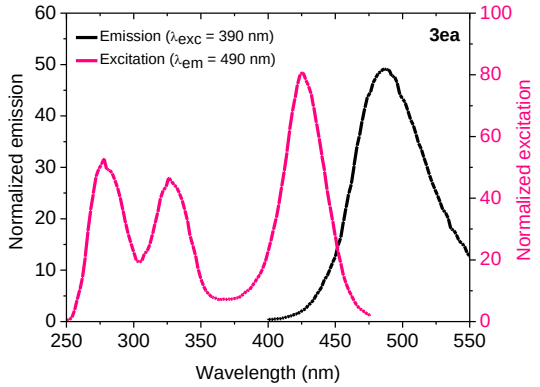

(c)

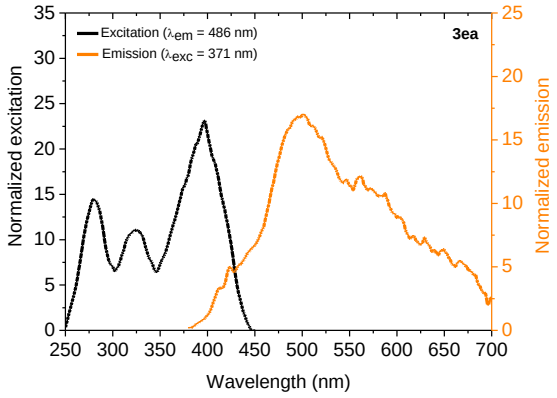

Figure S9. Steady-state emission fluorescence spectra of compound **3ea** in **(a)** $CHCl_3$, **(b)** DMSO and **(c)** MeOH ([ ] = 1.50 x 10^{-5} M).

(a)

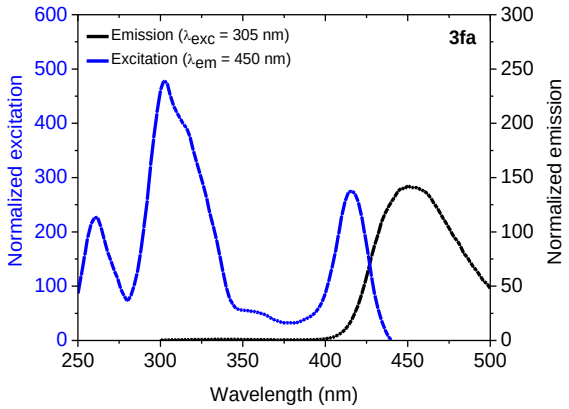

(b)

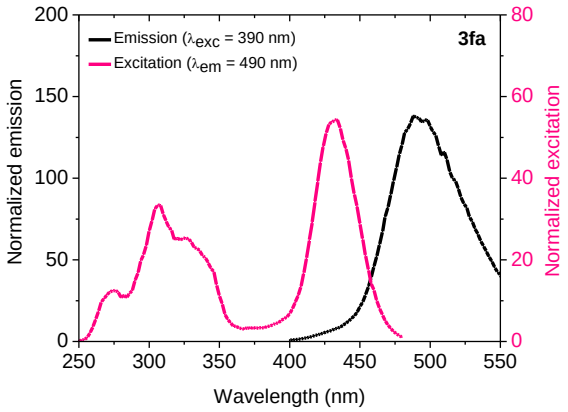

(c)

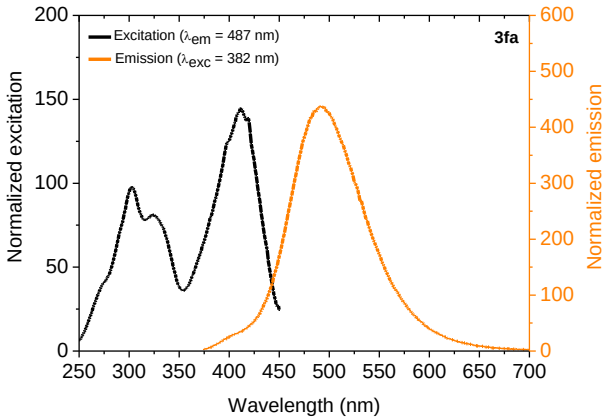

Figure S10. Steady-state emission fluorescence spectra of compound **3fa** in **(a)** $CHCl_3$, **(b)** DMSO and **(c)** MeOH ([ ] = 1.50 x 10^{-5} M).

(a)

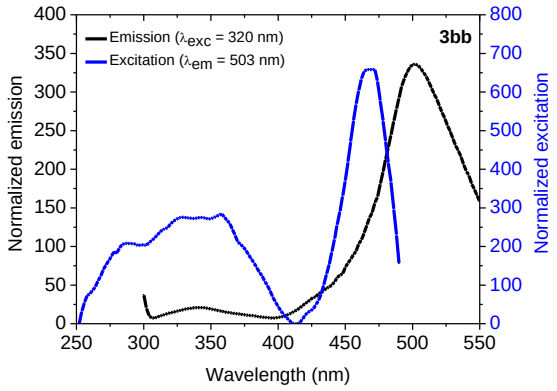

(b)

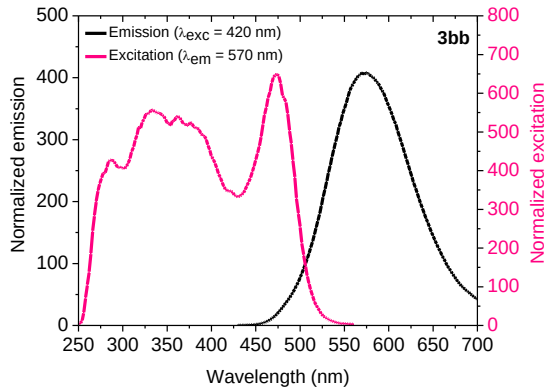

(c)

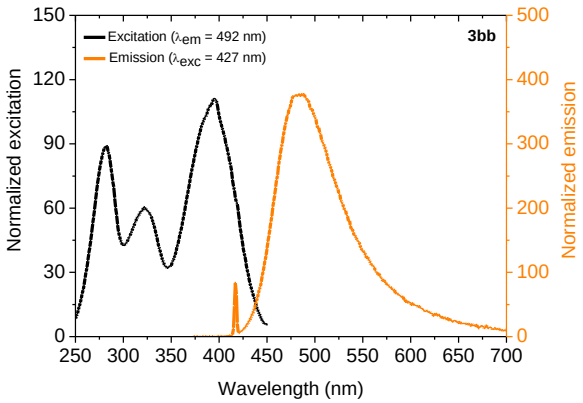

Figure S11. Steady-state emission fluorescence spectra of compound **3bb** in **(a)** $CHCl_3$, **(b)** DMSO and **(c)** MeOH ([ ] = 1.50 x 10^{-5} M).

(a)

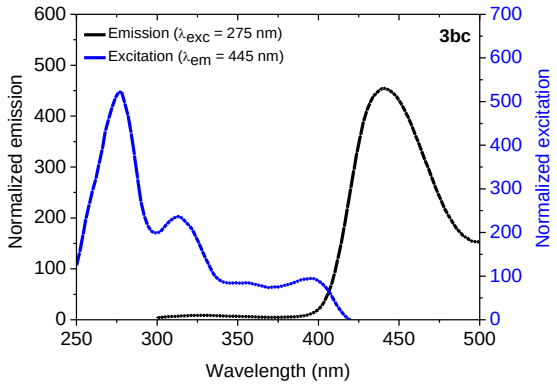

(b)

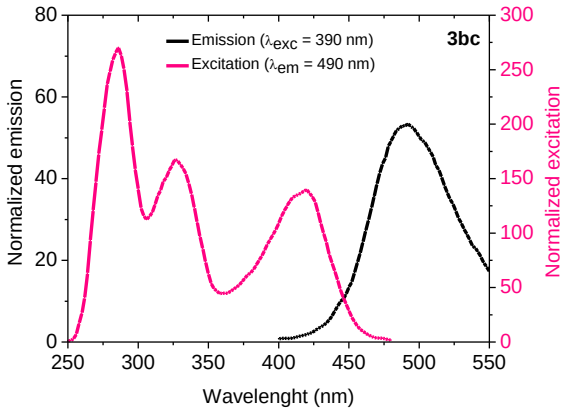

(c)

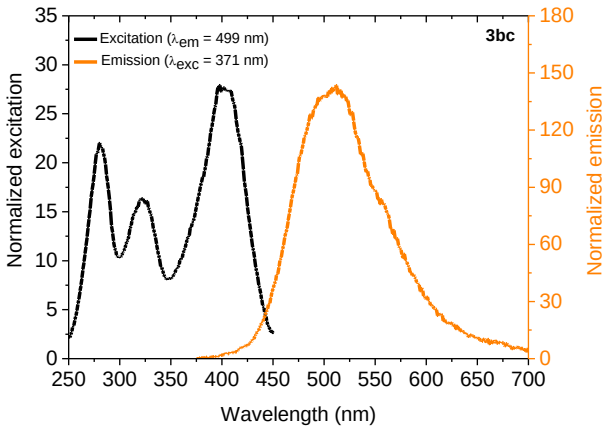

Figure S12. Steady-state emission fluorescence spectra of compound **3bc** in **(a)** $CHCl_3$, **(b)** DMSO and **(c)** MeOH ([ ] = 1.50 x 10^{-5} M).

(a)

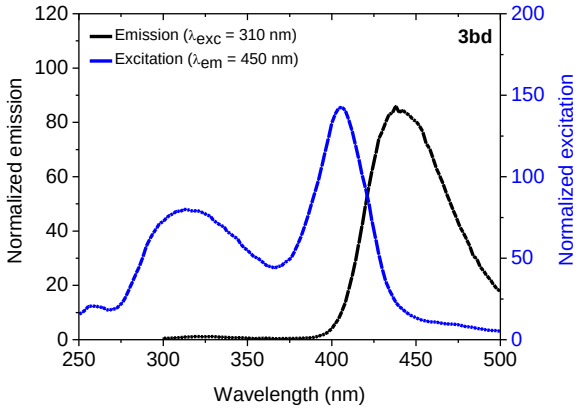

(b)

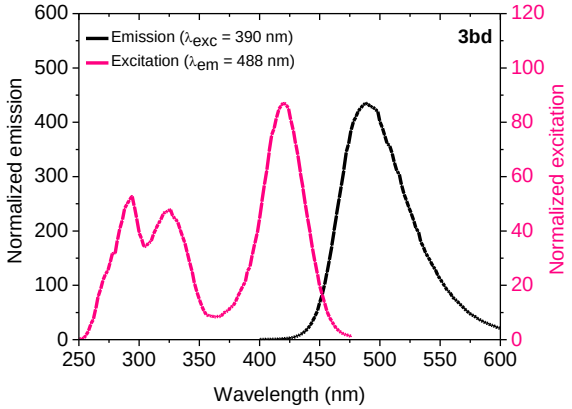

(c)

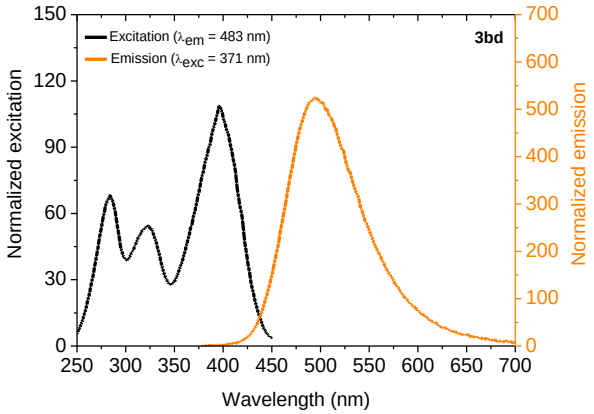

Figure S13. Steady-state emission fluorescence spectra of compound **3bd** in **(a)** $CHCl_3$, **(b)** DMSO and **(c)** MeOH ([ ] = 1.50 x 10^{-5} M).

(a)

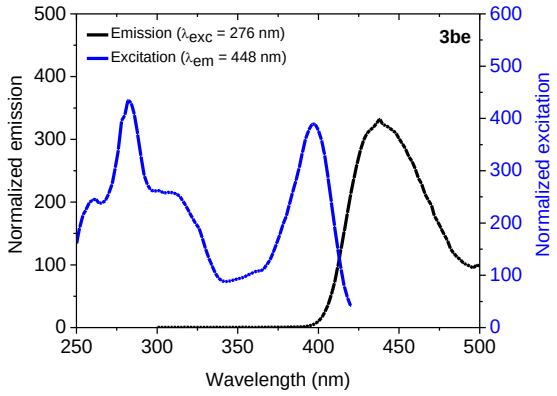

(b)

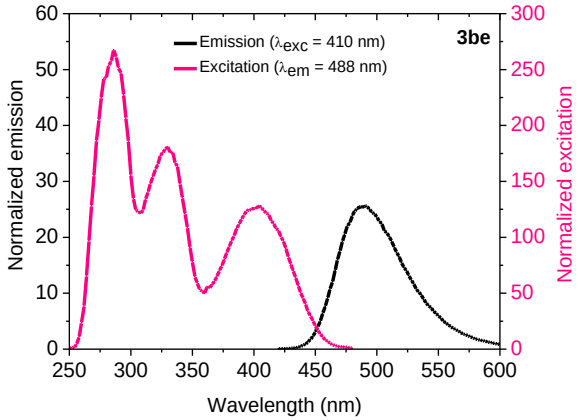

(c)

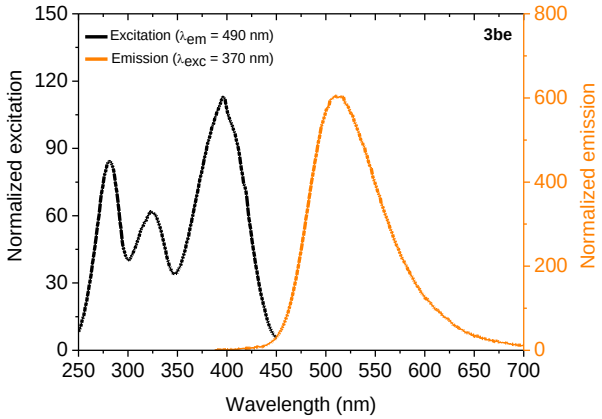

Figure S14. Steady-state emission fluorescence spectra of compound **3be** in **(a)** $CHCl_3$, **(b)** DMSO and **(c)** MeOH ([ ] = 1.50 x 10^{-5} M).

3. Singlet oxygen quantum yield (Φ_Δ) measurements

In a typical experiment of 1,3-diphenylisobenzofuran (DPBF) singlet oxygen quencher photo-oxidation [6], solutions containing DPBF (50 µM) with or without porphyrin derivatives 0.50 µM were prepared in DMSO in a quartz cuvette. In order to measure $^1O_2$ generation, UV-Vis spectra of the solutions (samples and standard) were recorded for different exposure times by using a 660 nm red diode laser positioned 2.0 cm from the sample (TheraLase DMC, São Carlos, SP, Brazil) with an average power of 100 mW, during 10 min (irradiation intervals every 30 s). The singlet oxygen production quantum yield (Φ_Δ) was calculated by using Equation (3):

$$\Phi_\Delta = \Phi_\Delta^{std} \frac{k}{k^{std}} \frac{I^{std}}{I} \quad \textbf{(3)}$$

in which, $I^{std} / I = (1 – 10^{Astd}) / (1 – 10^{A})$, Φ_Δ^{std} is the singlet oxygen quantum yield of standard sample (in our case, methylene blue (MB) in ethanol solution, $\Phi_\Delta^{std} = 0.52$) [7], k and k^{std} are the photo-oxidation kinetic constants for the Schiff bases and MB (standard), respectively, and A^{std} and A are the absorbances of MB and studied compounds, respectively.

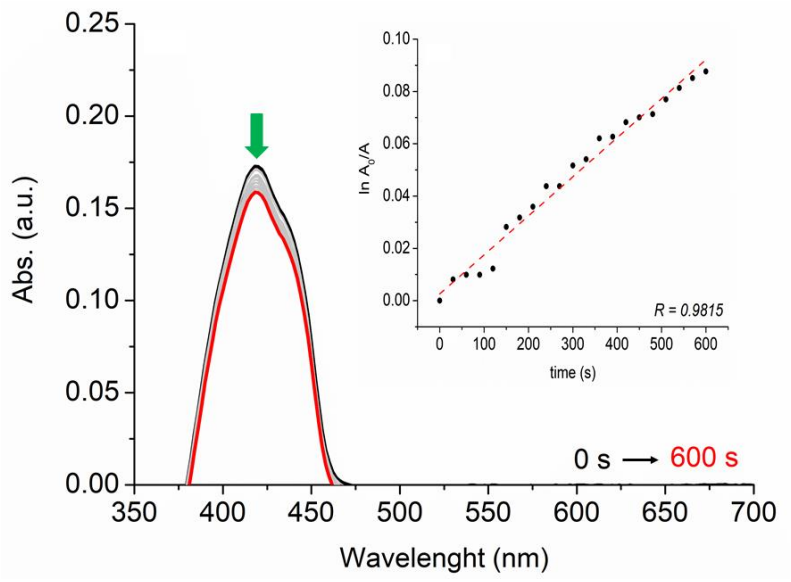

Figure S15. Photo-oxidation of DPBF by red-light irradiation with diode laser (λ = 660 nm) in the presence of compound **3aa**. The *inset* shows the first-order kinetic profile.

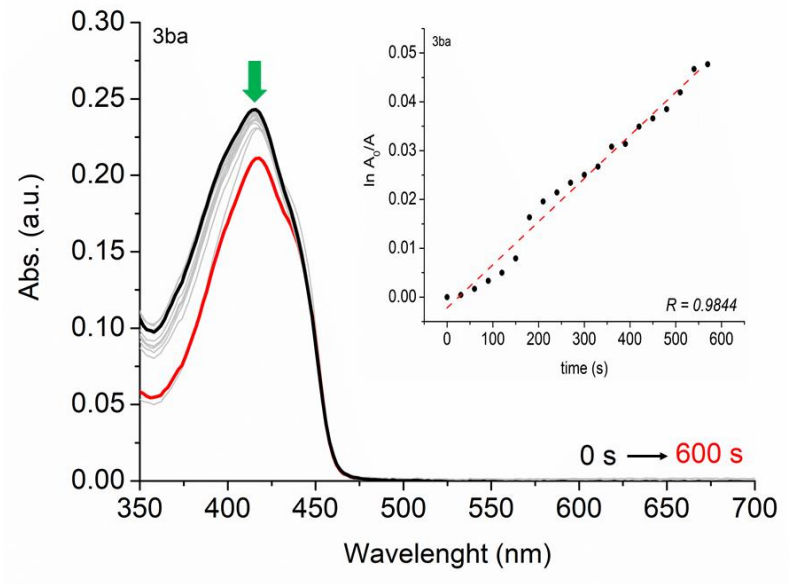

Figure S16. Photo-oxidation of DPBF by red-light irradiation with diode laser (λ = 660 nm) in the presence of compound **3ba**. The *inset* shows the first-order kinetic profile.

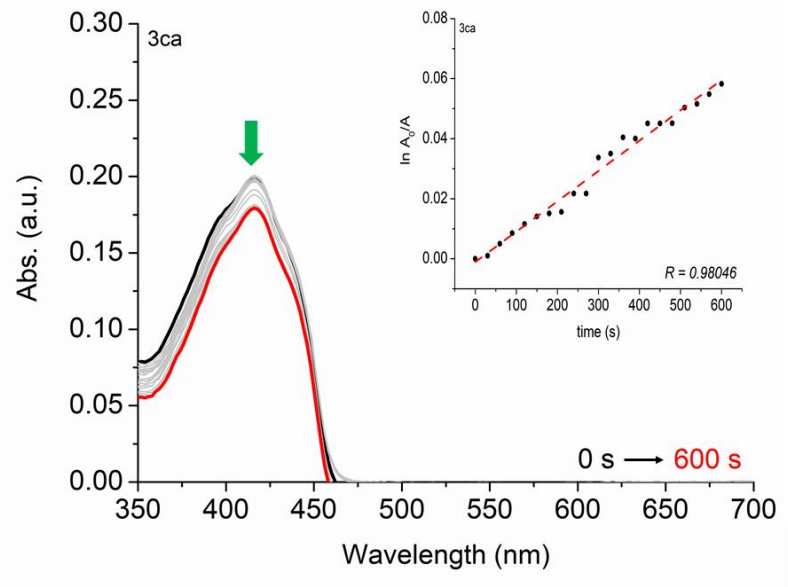

Figure S17. Photo-oxidation of DPBF by red-light irradiation with diode laser (λ = 660 nm) in the presence of compound **3ca**. The *inset* shows the first-order kinetic profile.

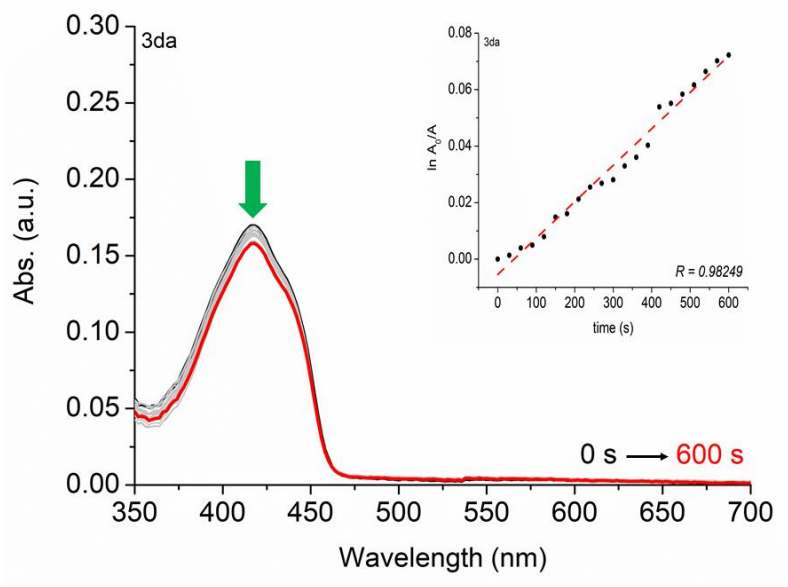

Figure S18. Photo-oxidation of DPBF by red-light irradiation with diode laser (λ = 660 nm) in the presence of compound **3da**. The *inset* shows the first-order kinetic profile.

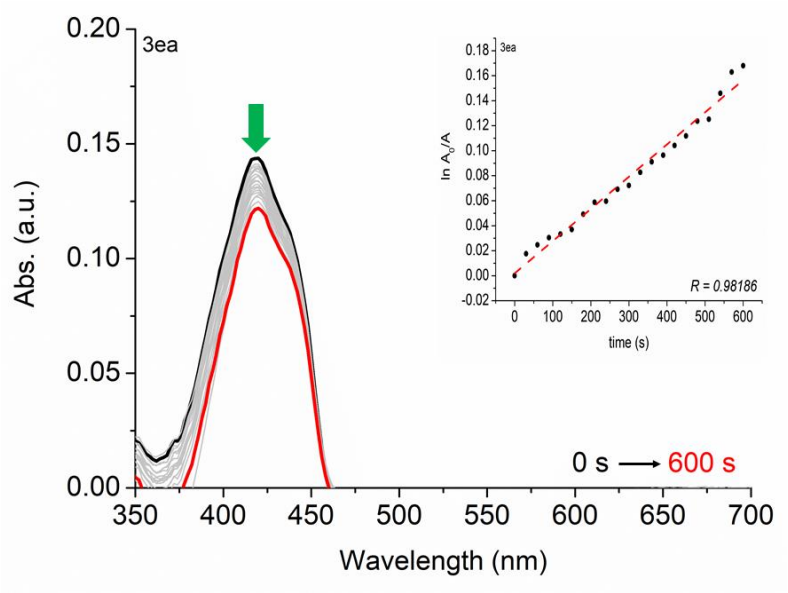

Figure S19. Photo-oxidation of DPBF by red-light irradiation with diode laser (λ = 660 nm) in the presence of compound **3ea**. The *inset* shows the first-order kinetic profile.

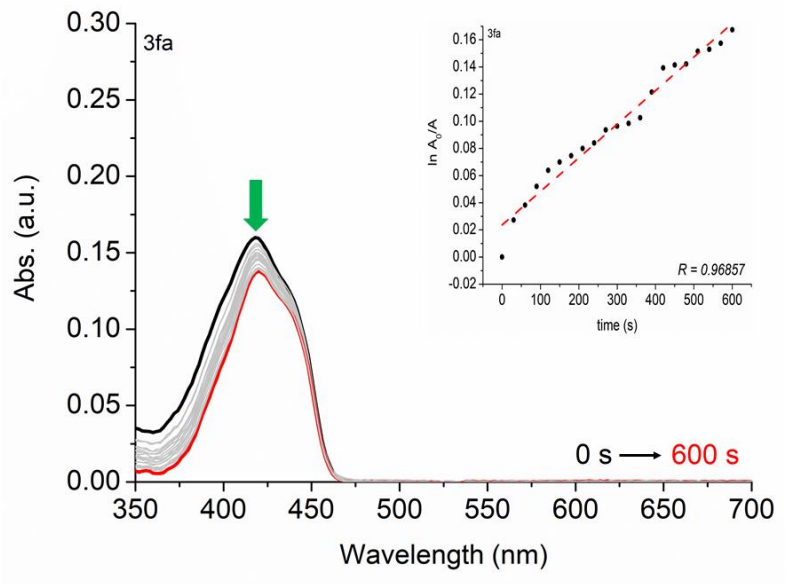

Figure S20. Photo-oxidation of DPBF by red-light irradiation with diode laser (λ = 660 nm) in the presence of compound **3fa**. The *inset* shows the first-order kinetic profile.

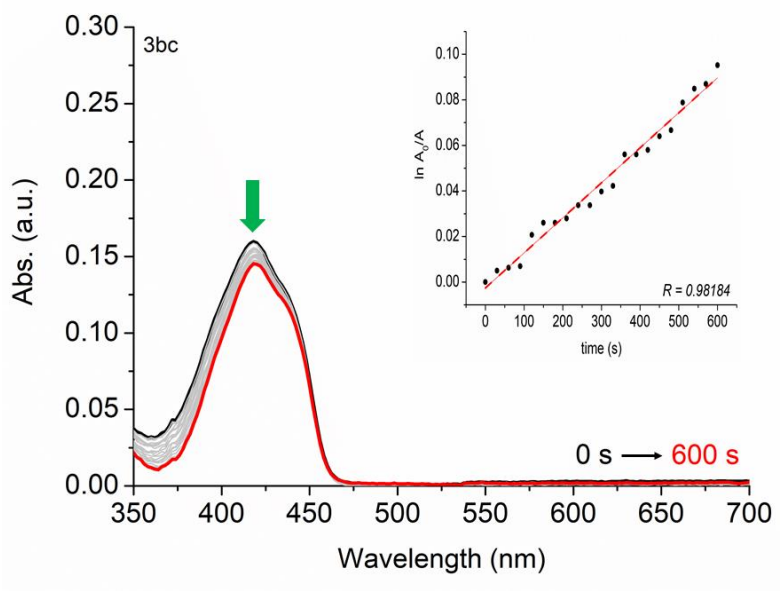

Figure S21. Photo-oxidation of DPBF by red-light irradiation with diode laser (λ = 660 nm) in the presence of compound **3bc**. The *inset* shows the first-order kinetic profile.

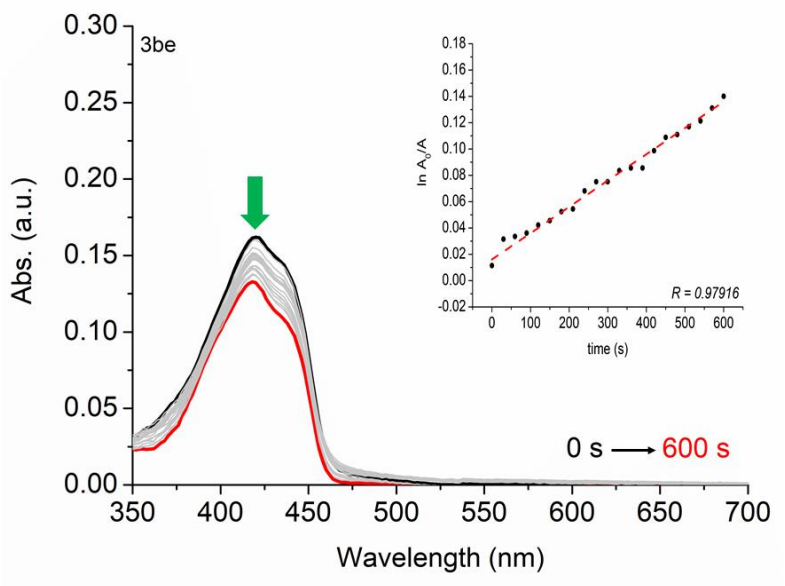

Figure S22. Photo-oxidation of DPBF by red-light irradiation with diode laser (λ = 660 nm) in the presence of compound **3bd**. The *inset* shows the first-order kinetic profile.

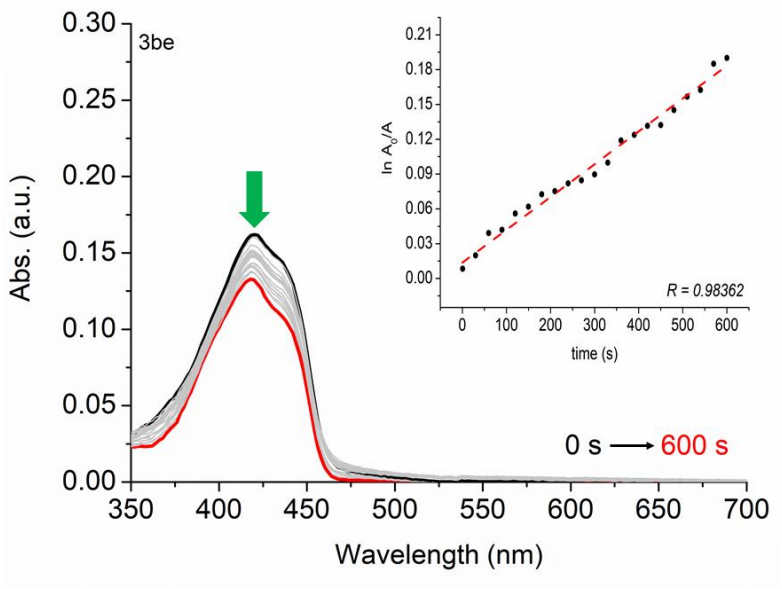

Figure 23. Photo-oxidation of DPBF by red-light irradiation with diode laser (λ = 660 nm) in the presence of compound **3be**. The *inset* shows the first-order kinetic profile.

4. ^{1}H, ^{13}C and ^{19}F NMR Spectra

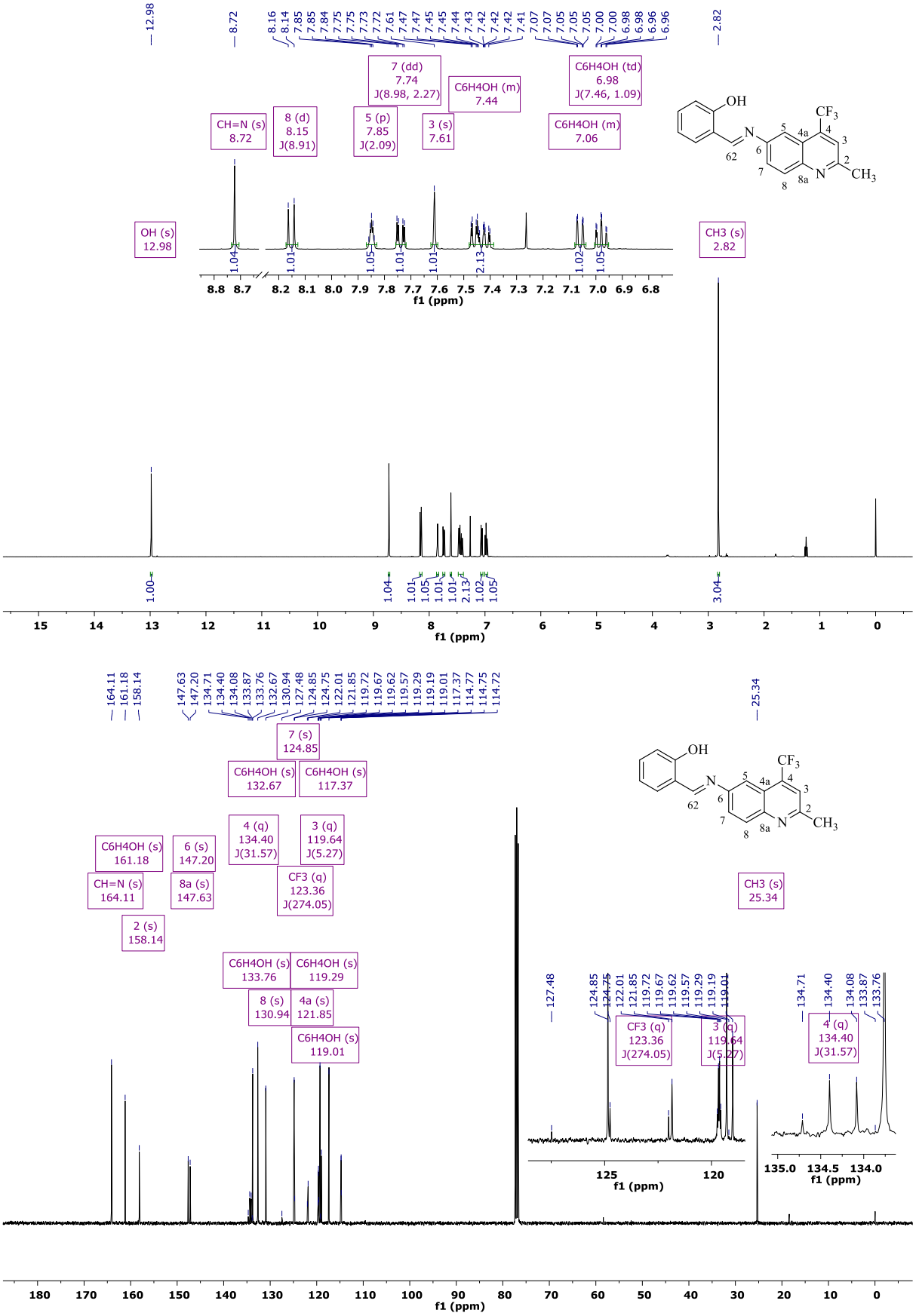

Figure S24. (a) ^{1}H (400 MHz) and (b) ^{13}C (100 MHz) NMR spectra of **3aa** in $CDCl_3$.

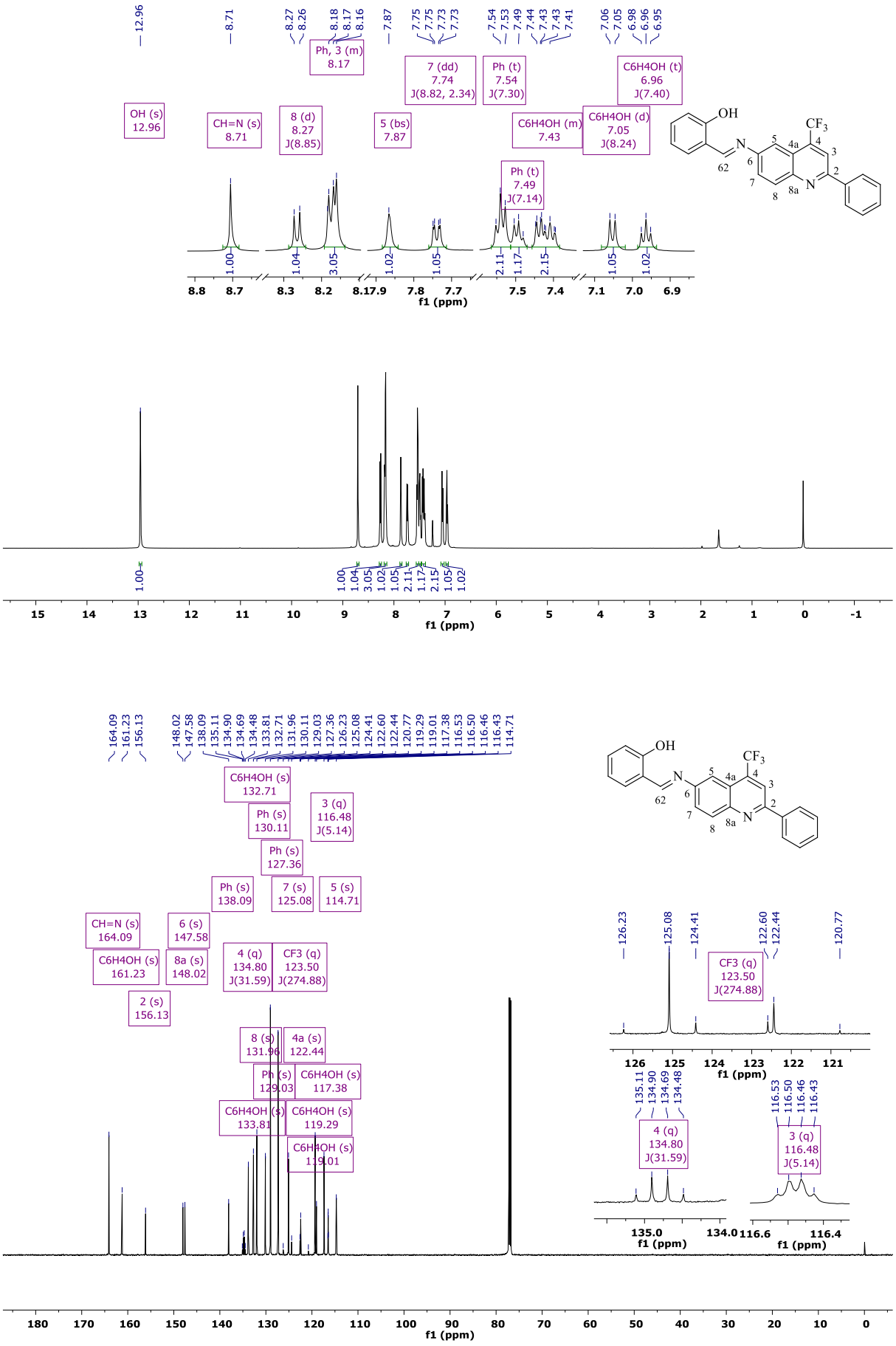

Figure S24. (a) ^{1}H (600 MHz) and (b) ^{13}C (151 MHz) NMR spectra of **3ba** in $CDCl_3$.

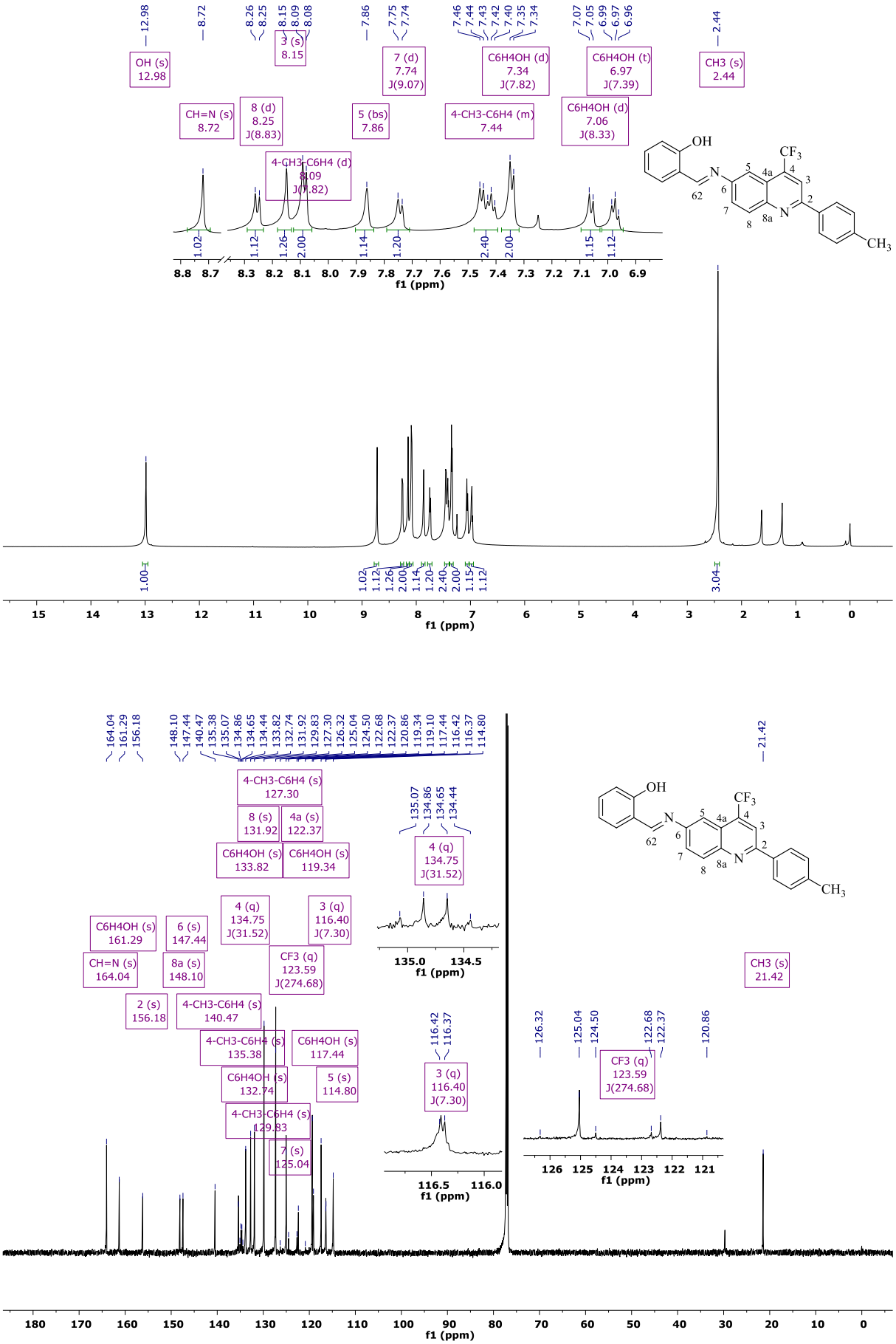

Figure S25. (a) ^{1}H (600 MHz) and (b) ^{13}C (151 MHz) NMR spectra of **3ca** in $CDCl_3$.

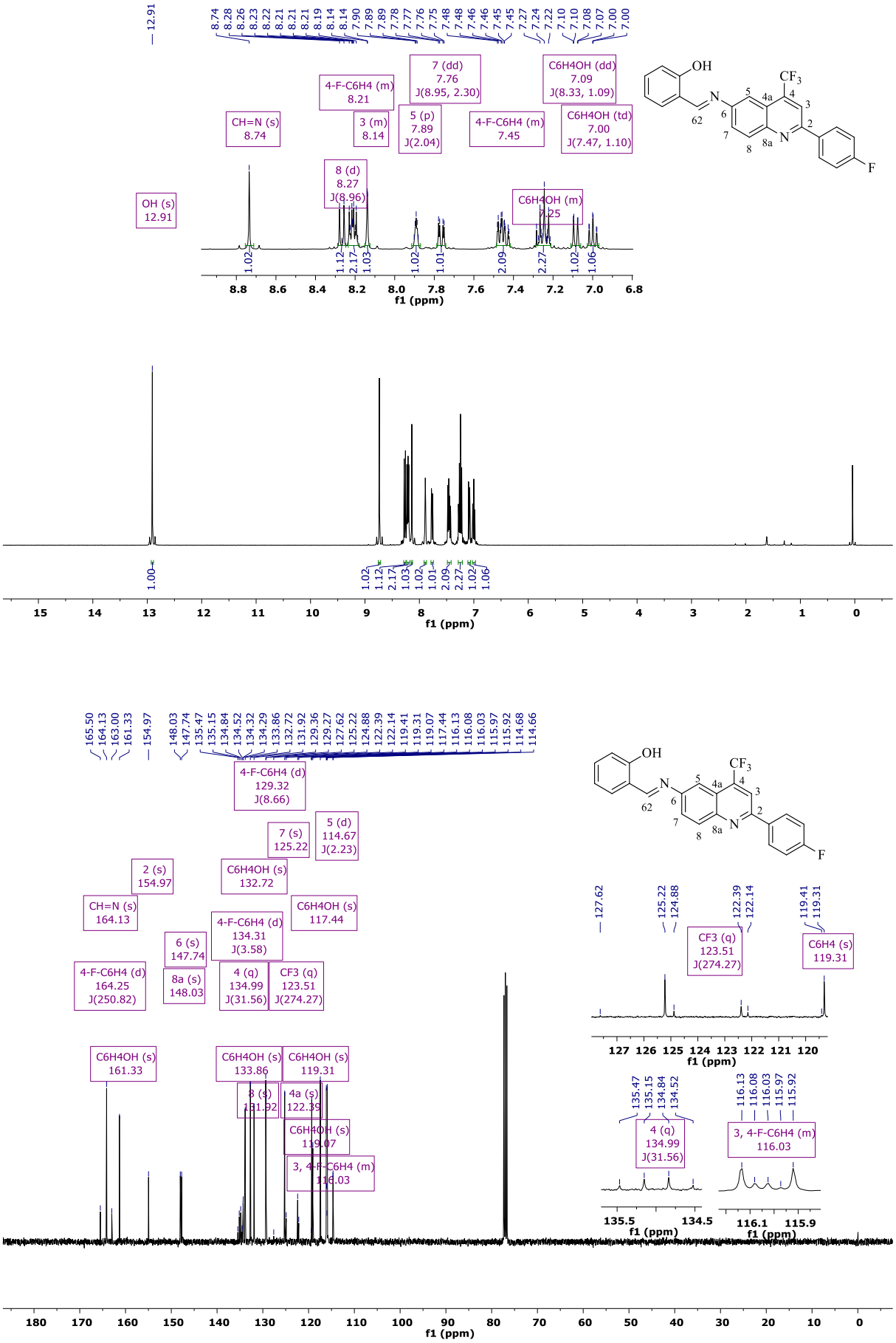

Figure S26. (a) ^{1}H (400 MHz) and (b) ^{13}C (100 MHz) NMR spectra of **3da** in $CDCl_3$.

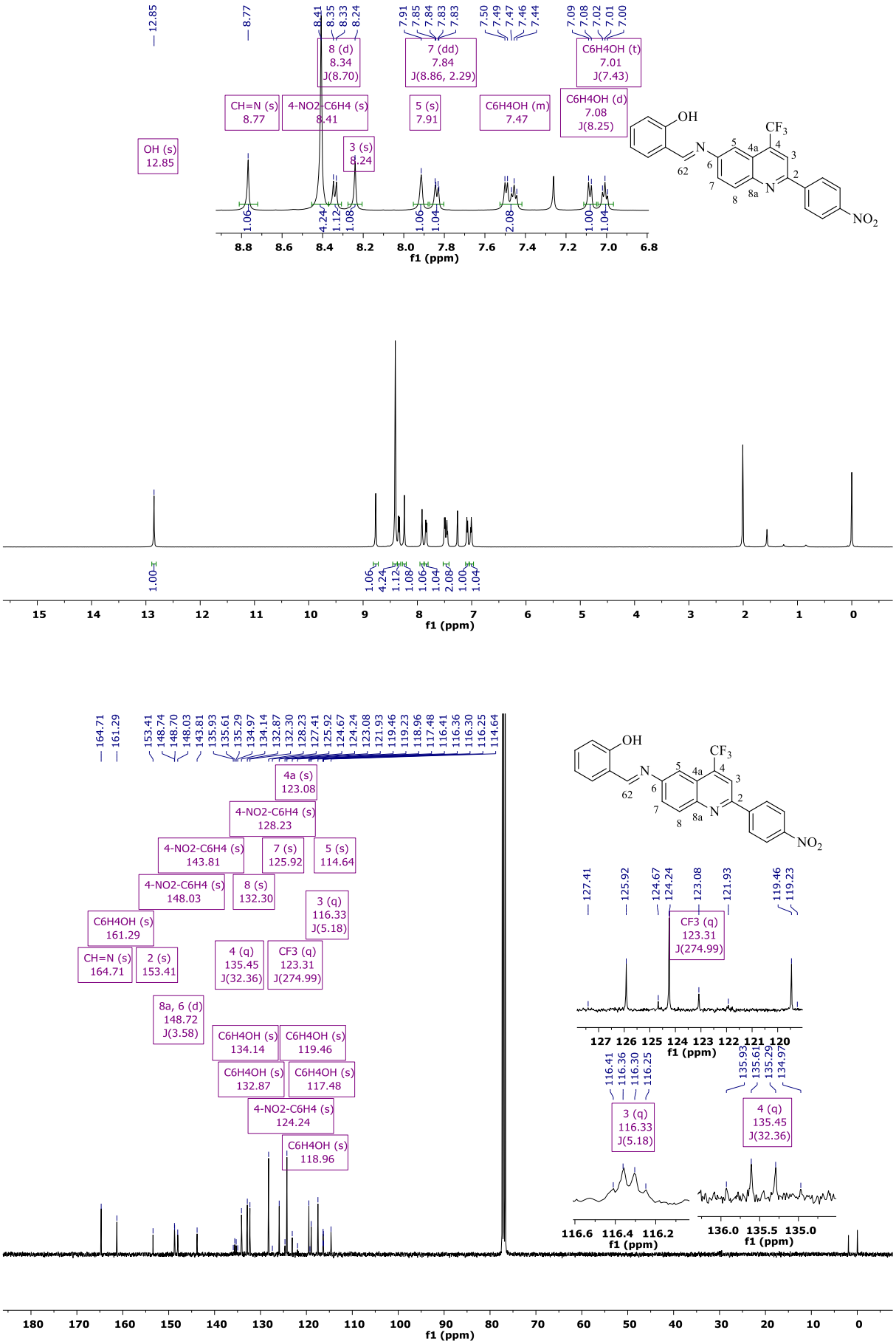

Figure S27. (a) ^{1}H (600 MHz) and (b) ^{13}C (100 MHz) NMR spectra of **3ea** in $CDCl_3$.

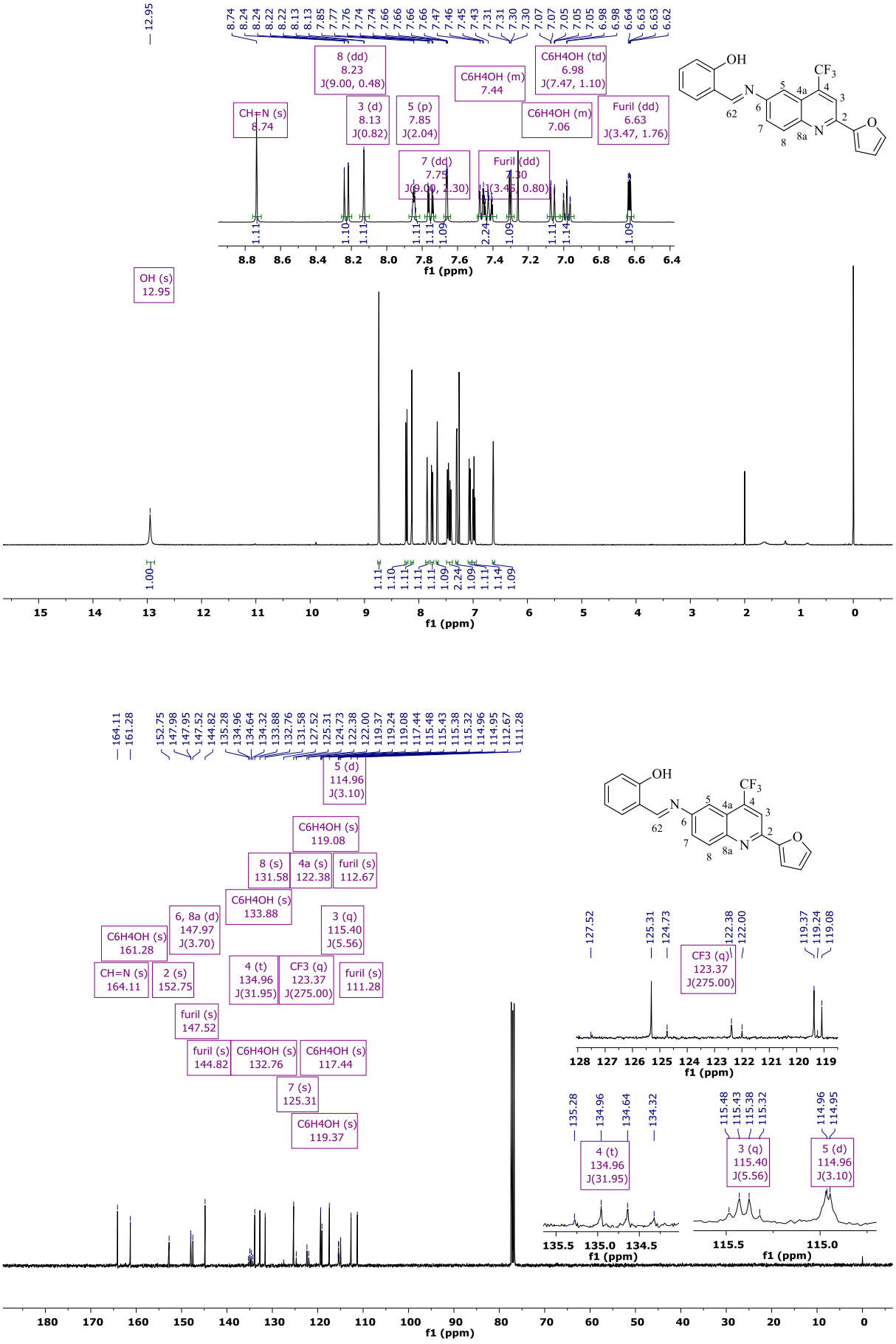

Figure S28. (a) ^{1}H (400 MHz) and (b) ^{13}C (100 MHz) NMR spectra of **3fa** in $CDCl_3$.

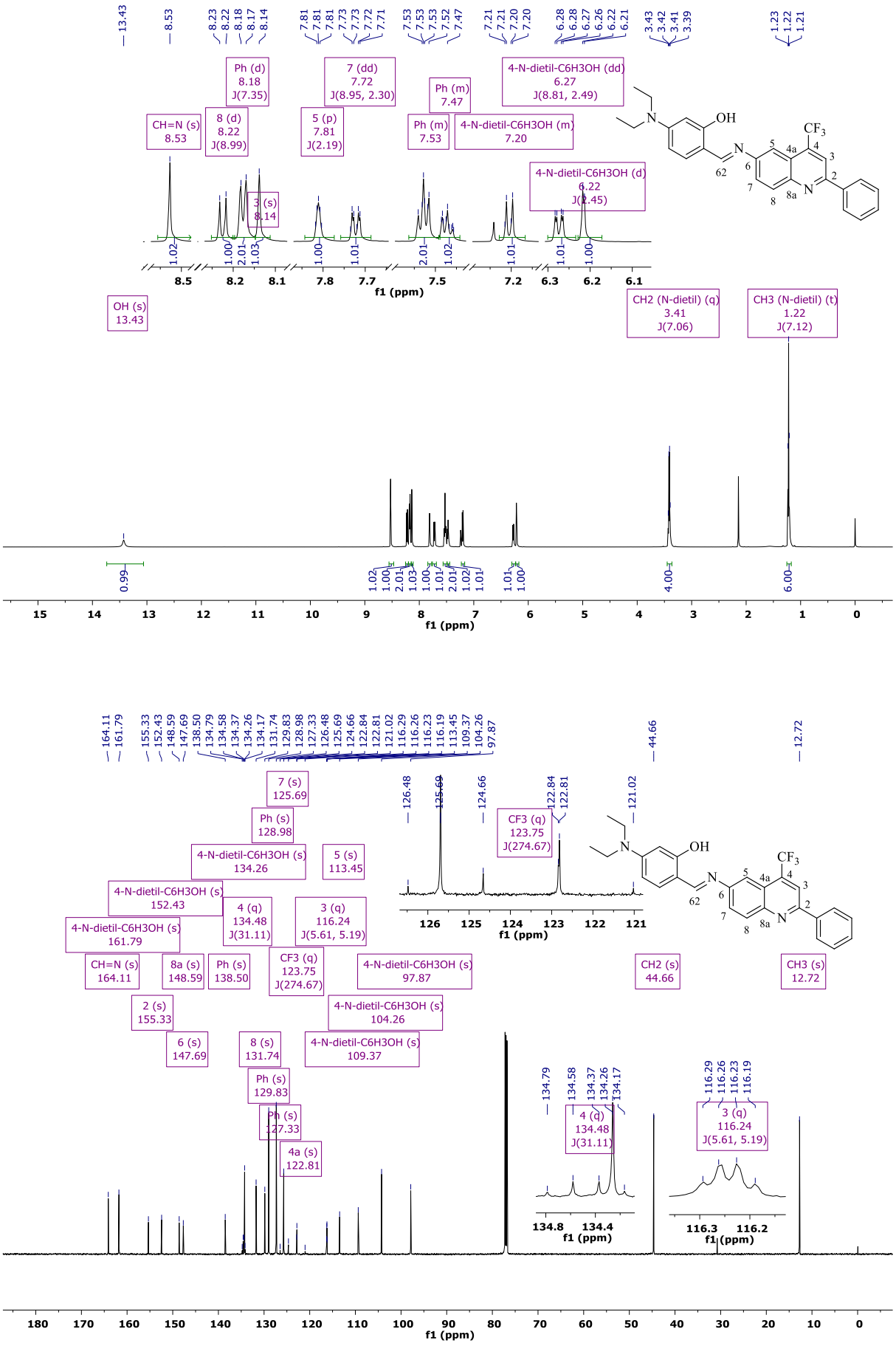

Figure S29. (a) ^{1}H (600 MHz) and (b) ^{13}C (151 MHz) NMR spectra of **3bb** in $CDCl_3$.

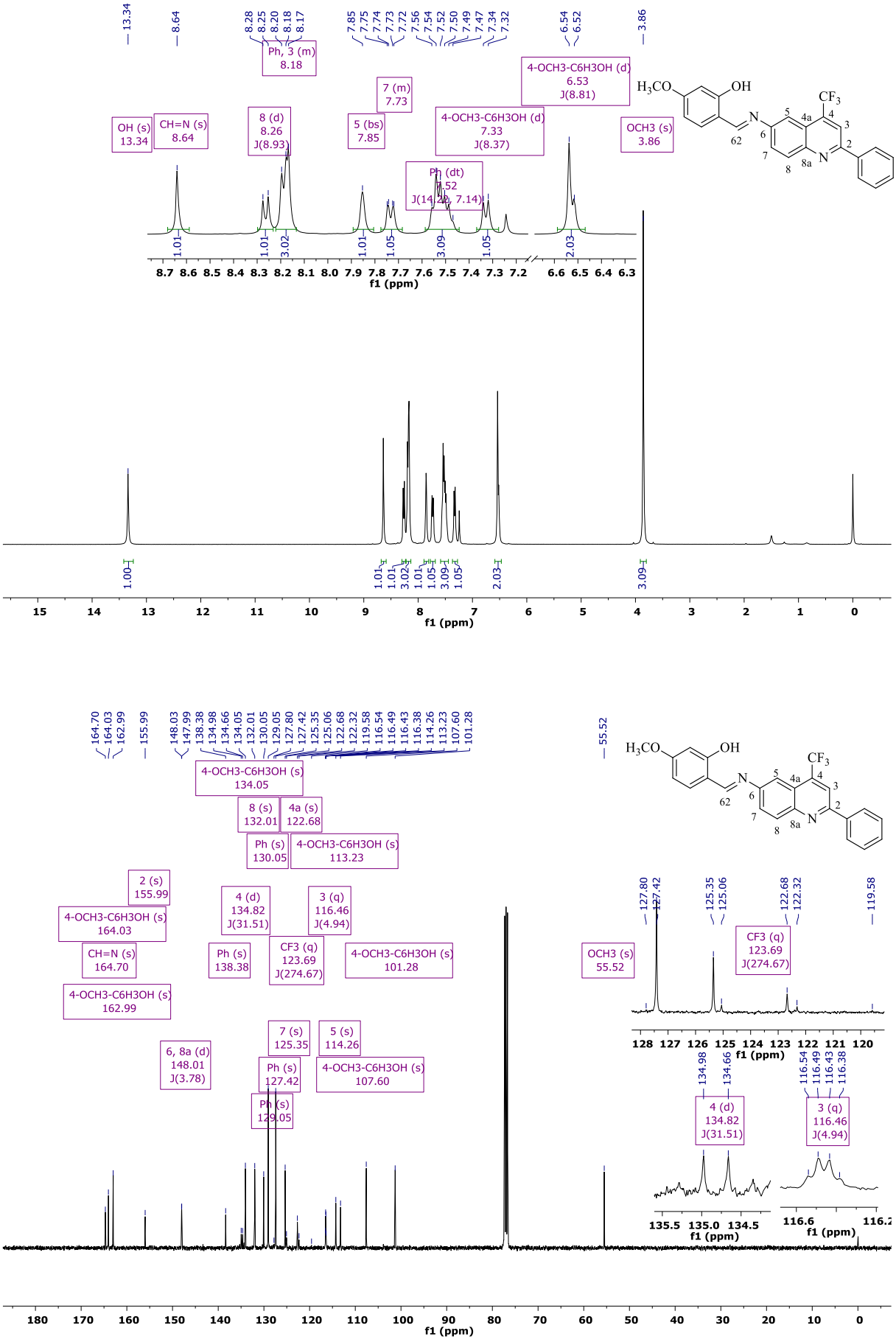

Figure S30. (a) ^{1}H (400 MHz) and (b) ^{13}C (100 MHz) NMR spectra of **3bc** in $CDCl_3$.

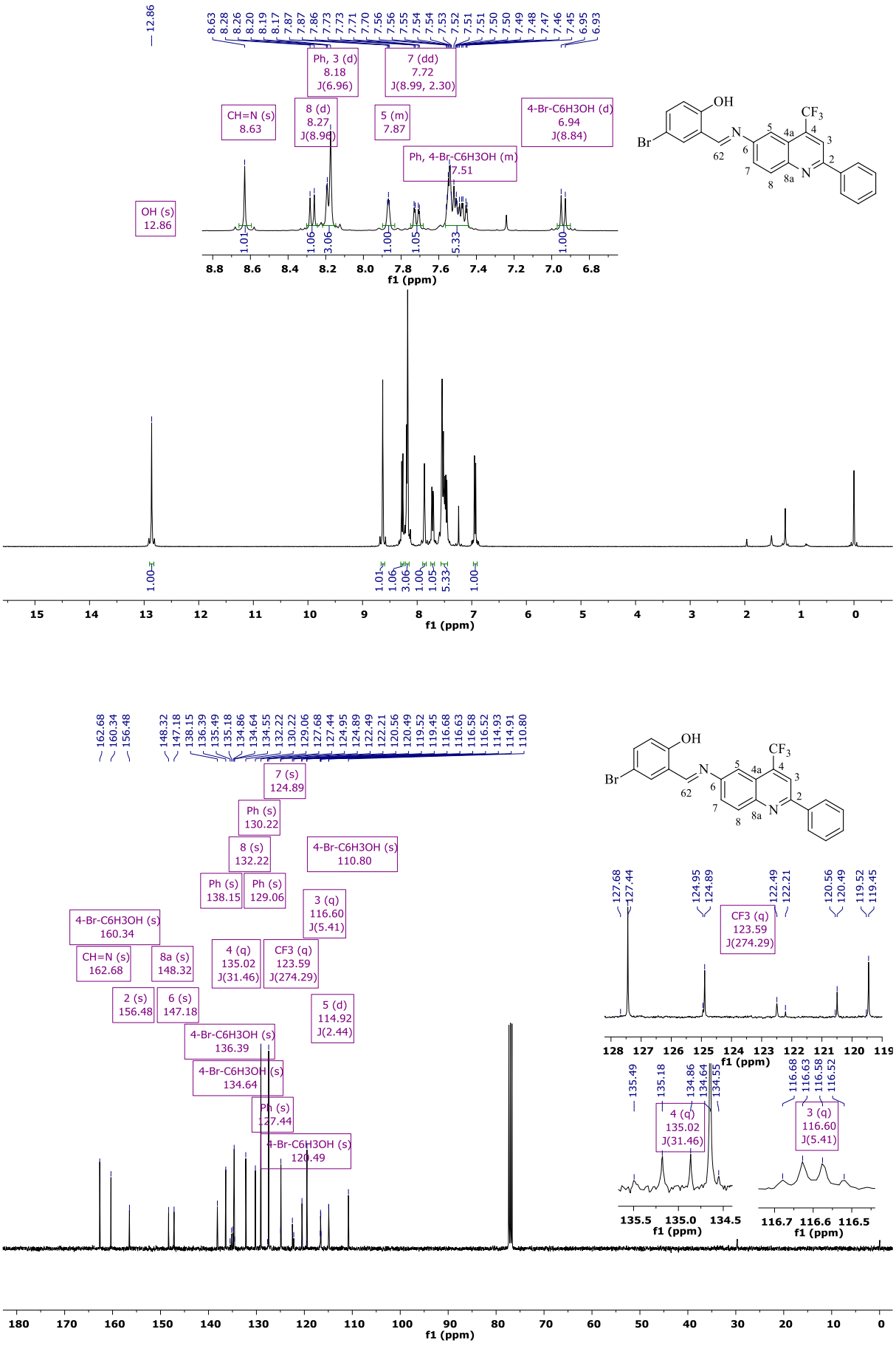

Figure S31. (a) ^{1}H (400 MHz) and (b) ^{13}C (100 MHz) NMR spectra of 3**bd** in $CDCl_3$.

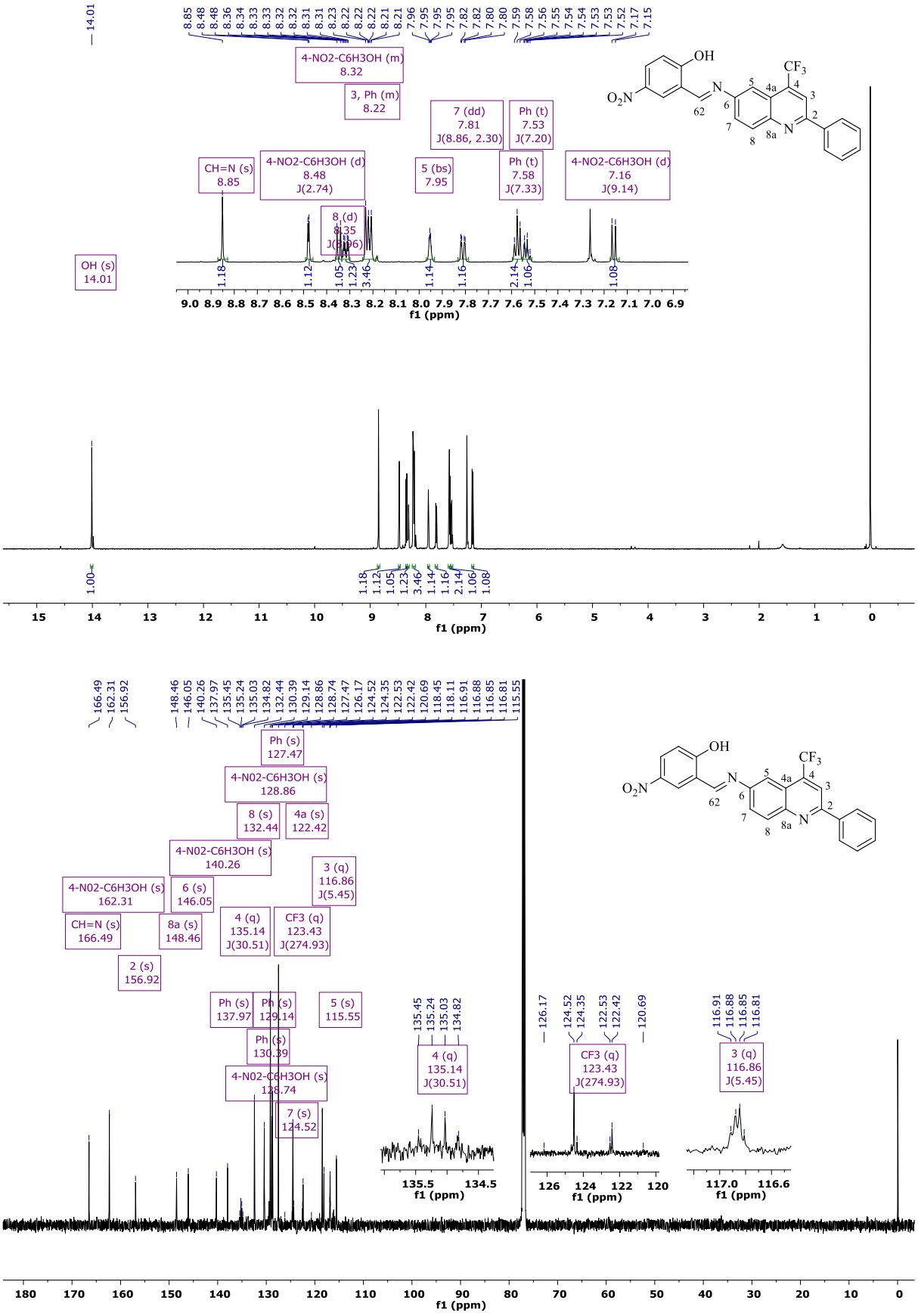

Figure S32. (a) ^{1}H (600 MHz) and (b) ^{13}C (151 MHz) NMR spectra of **3be** in $CDCl_3$.

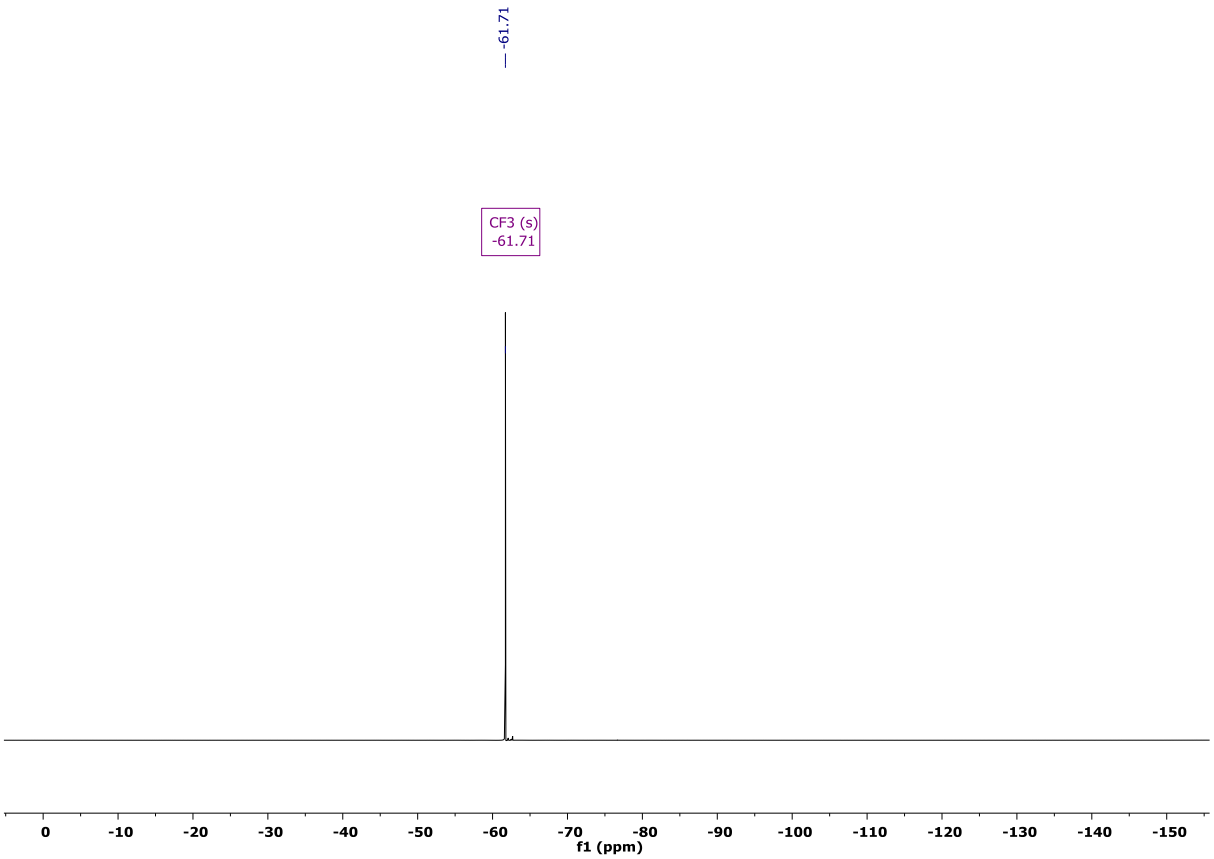

Figure S33. ^{19}F (565 MHz) NMR spectrum of **3aa** in $CDCl_3$.

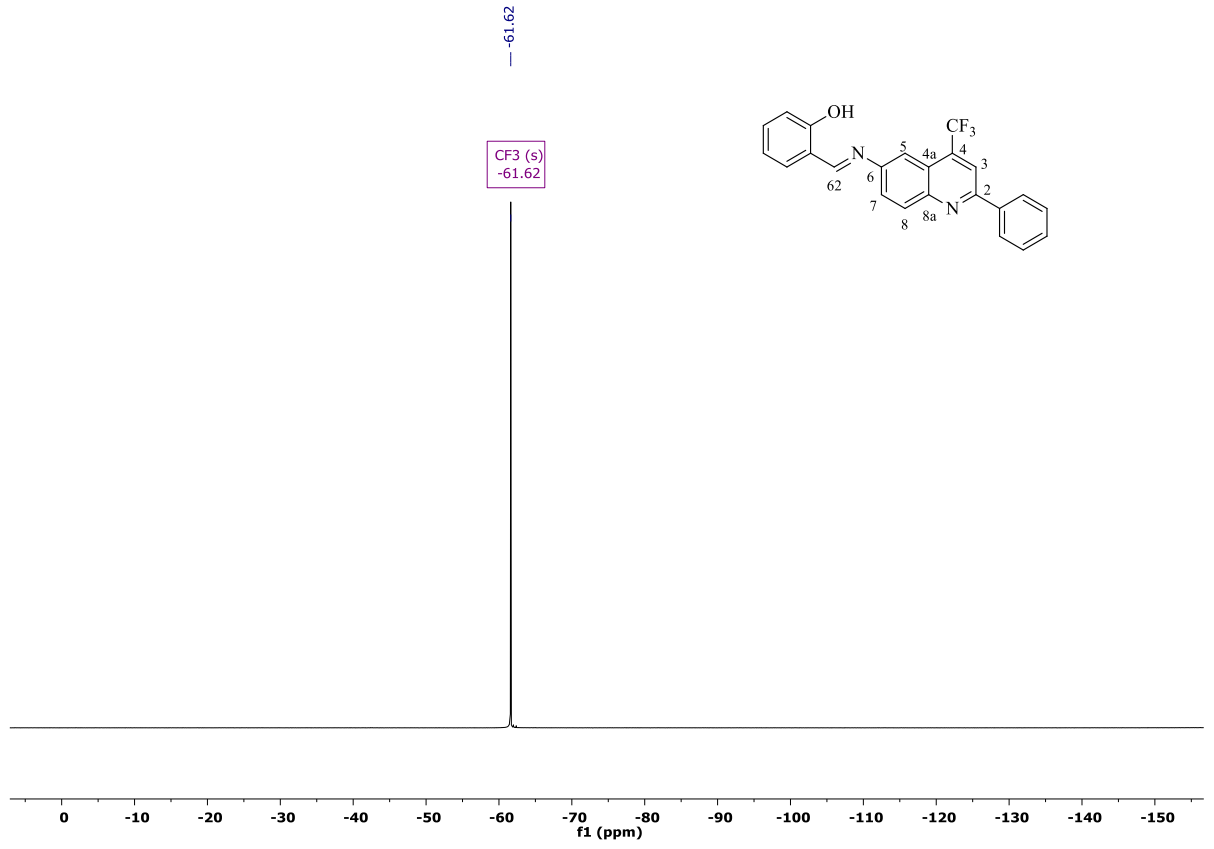

Figure S34. ^{19}F (565 MHz) NMR spectrum of **3ba** in $CDCl_3$.

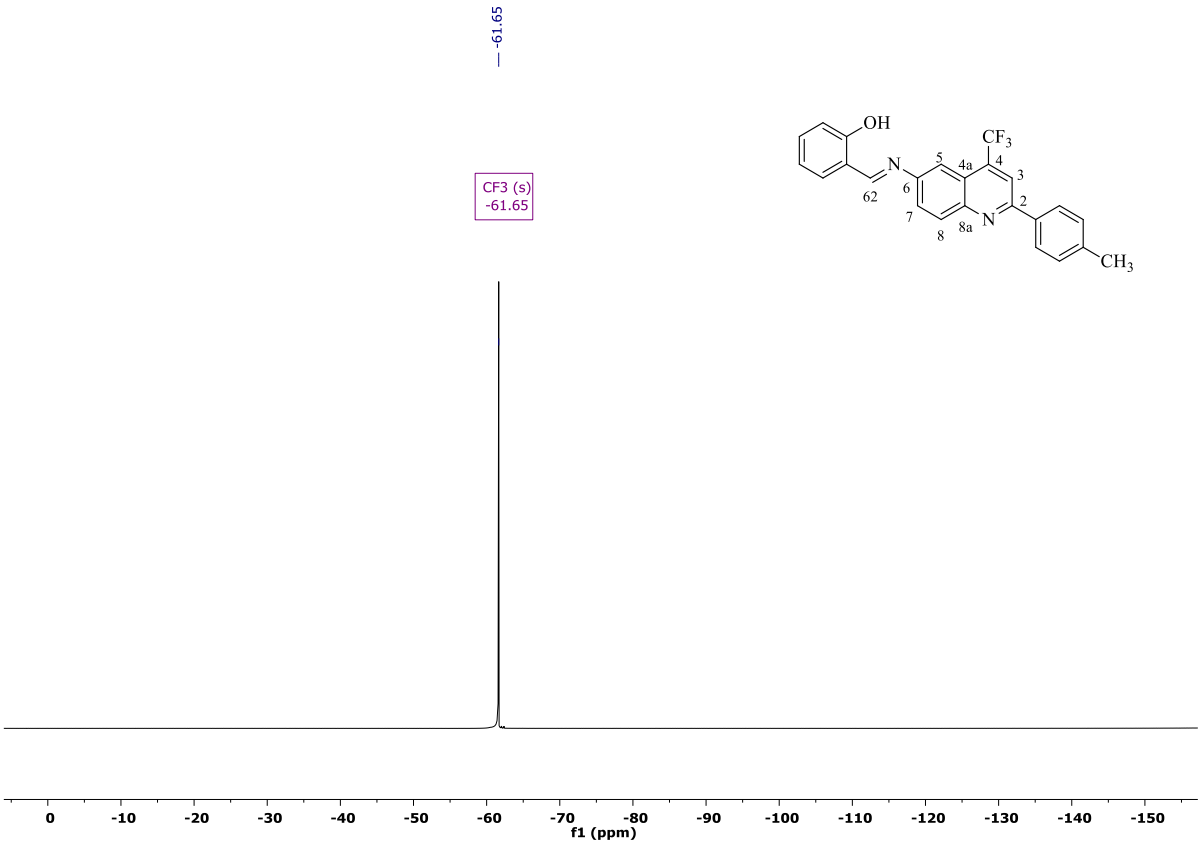

Figure S35. ^{19}F (565 MHz) NMR spectrum of **3ca** in $CDCl_3$.

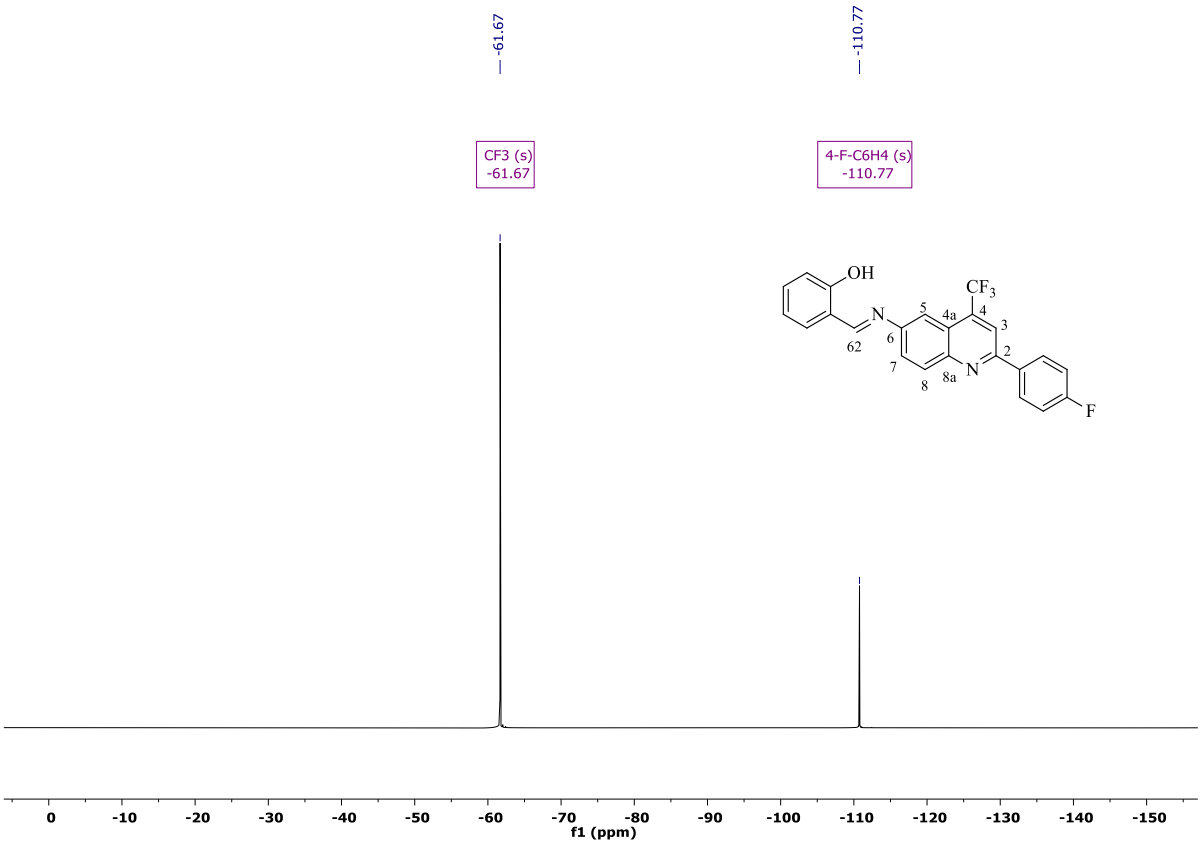

Figure S36. ^{19}F (565 MHz) NMR spectrum of **3da** in $CDCl_3$.

Figure S37. ^{19}F (565 MHz) NMR spectrum of **3ea** in $CDCl_3$.

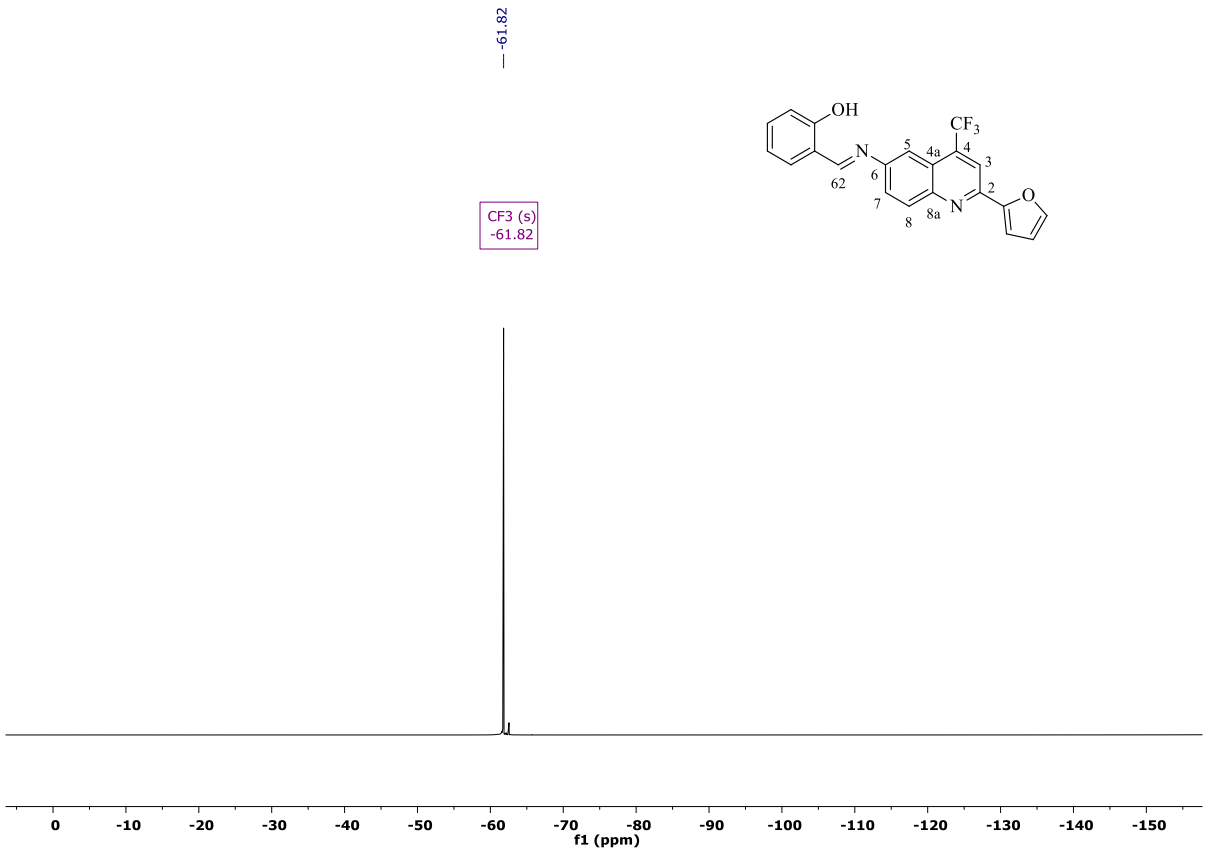

Figure S38. ^{19}F (565 MHz) NMR spectrum of **3fa** in $CDCl_3$.

Figure S39. ^{19}F (565 MHz) NMR spectrum of **3bb** in $CDCl_3$.

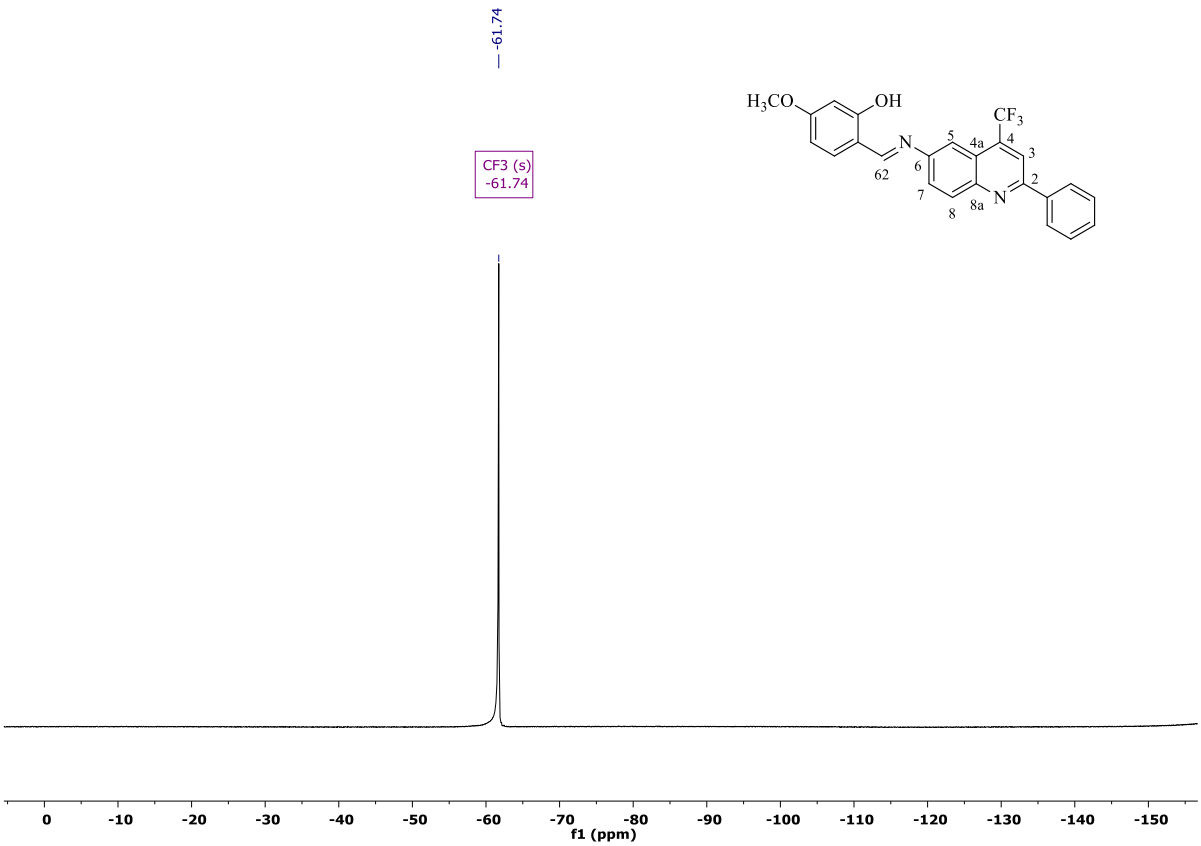

Figure S40. ^{19}F (565 MHz) NMR spectrum of **3bc** in $CDCl_3$.

Figure S41. ^{19}F (565 MHz) NMR spectrum of 3**bd** in $CDCl_3$.

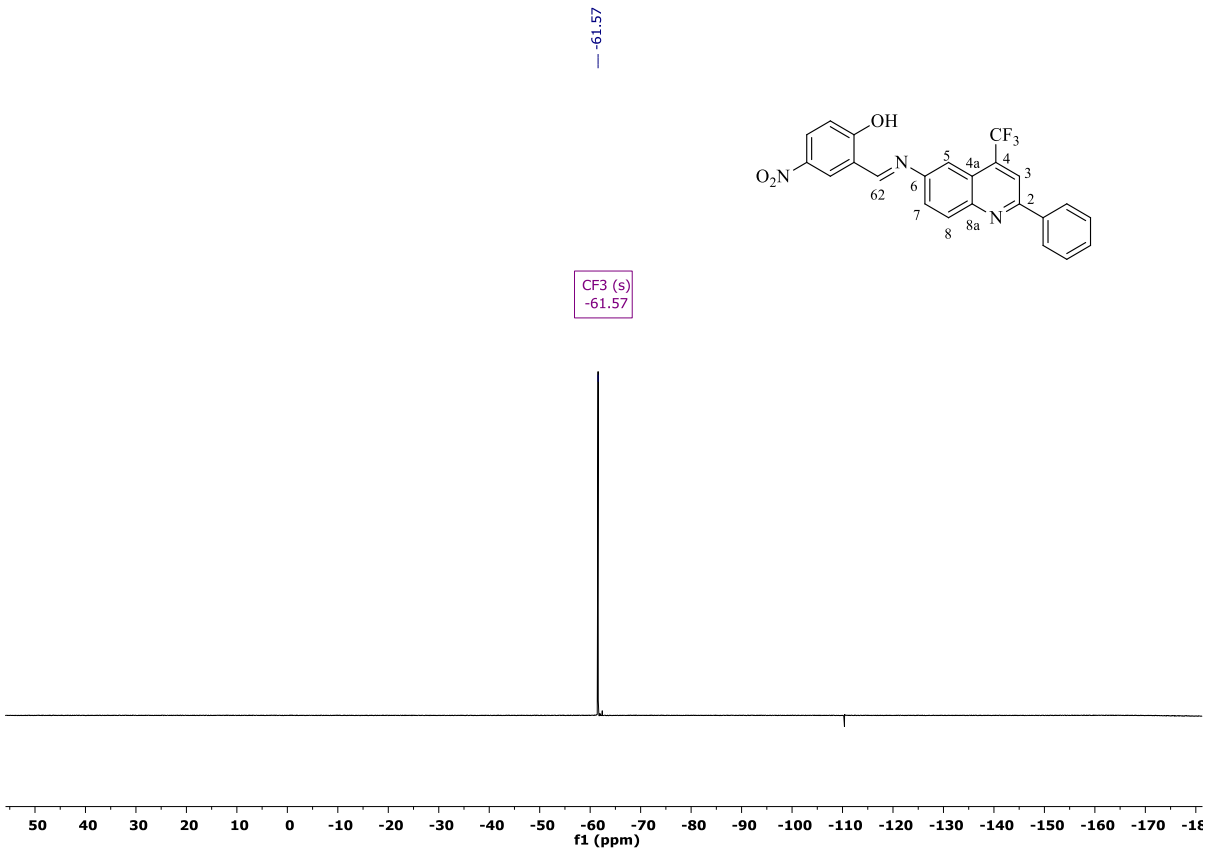

Figure S42. ^{19}F (565 MHz) NMR spectrum of **3be** in $CDCl_3$.

5. FT-IR Spectra

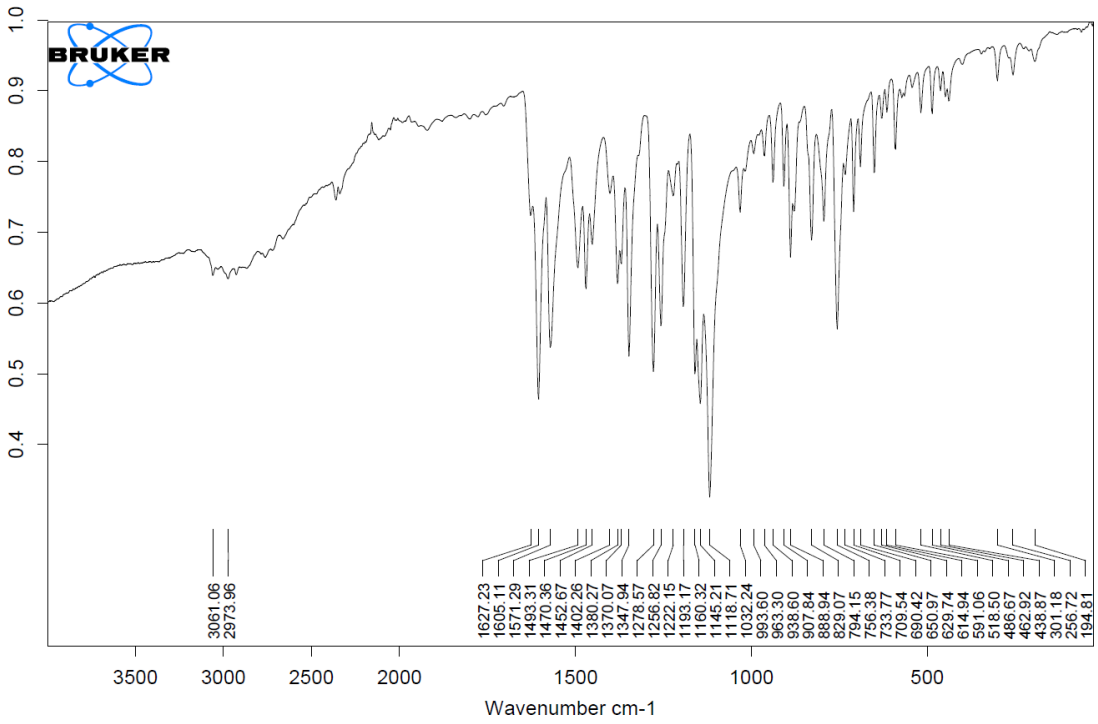

Figure S44. FT-IR spectrum of compound **3aa**.

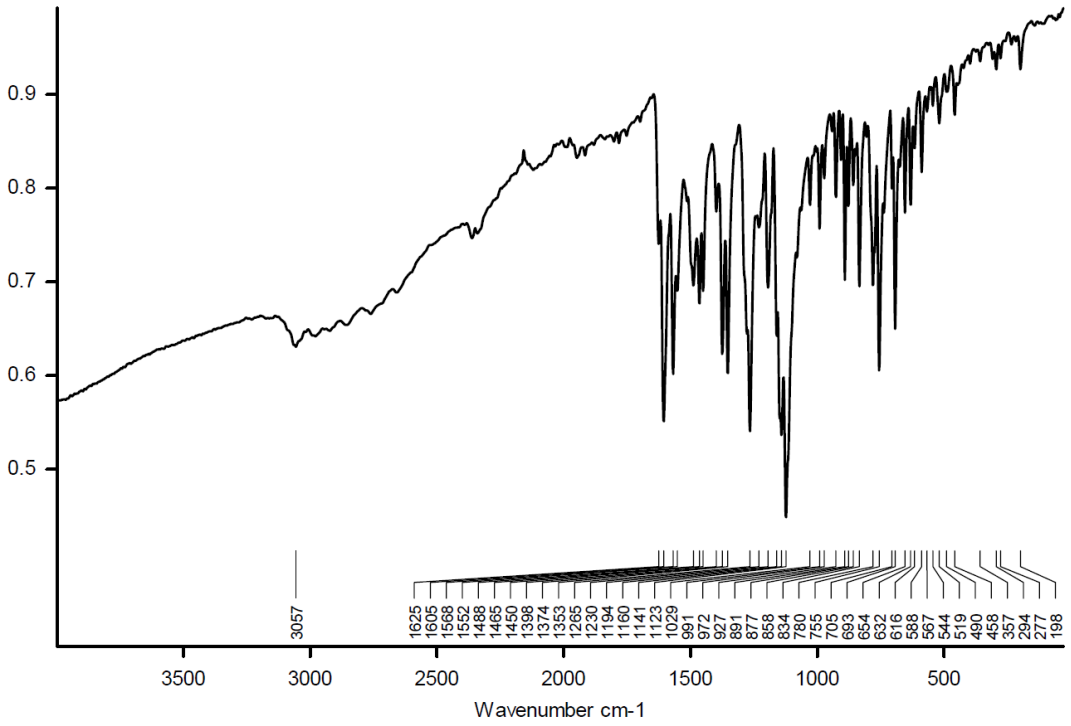

Figure S45. FT-IR spectrum of compound **3ba**.

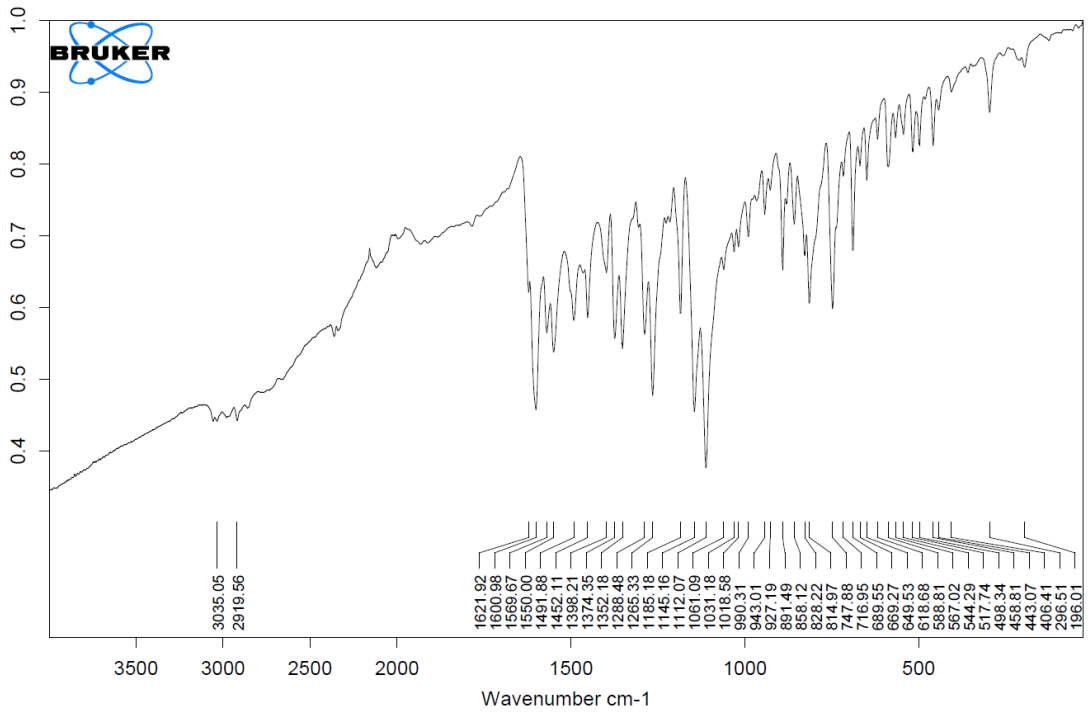

Figure S436. FT-IR spectrum of compound **3ca**.

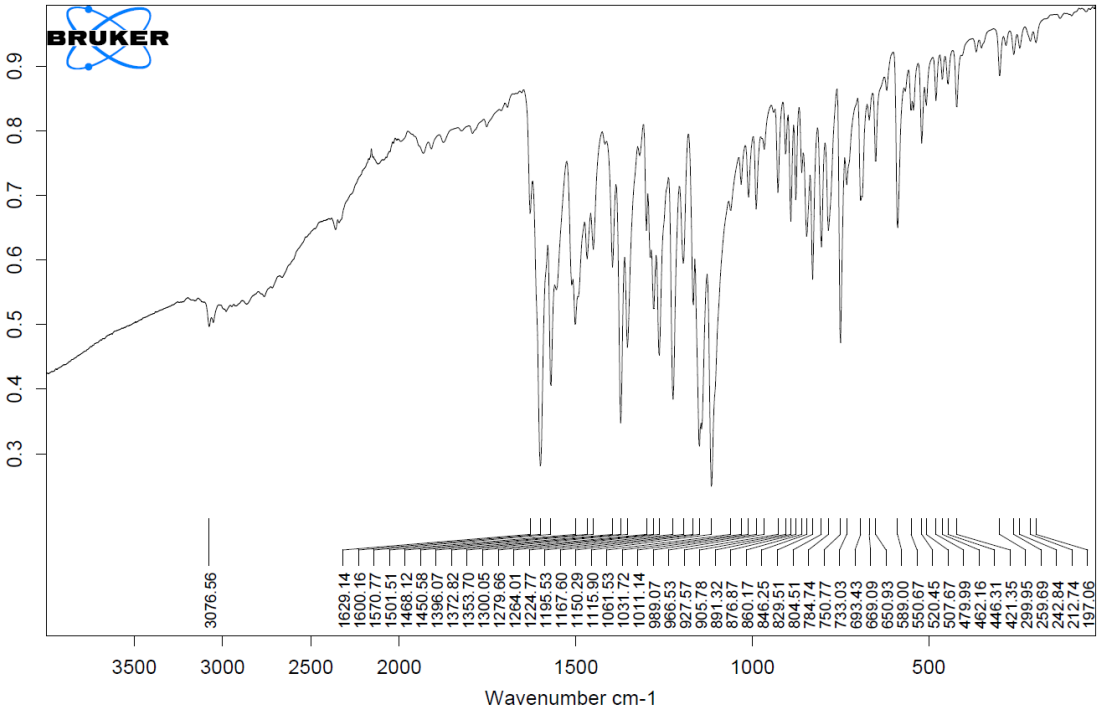

Figure S47. FT-IR spectrum of compound **3da**.

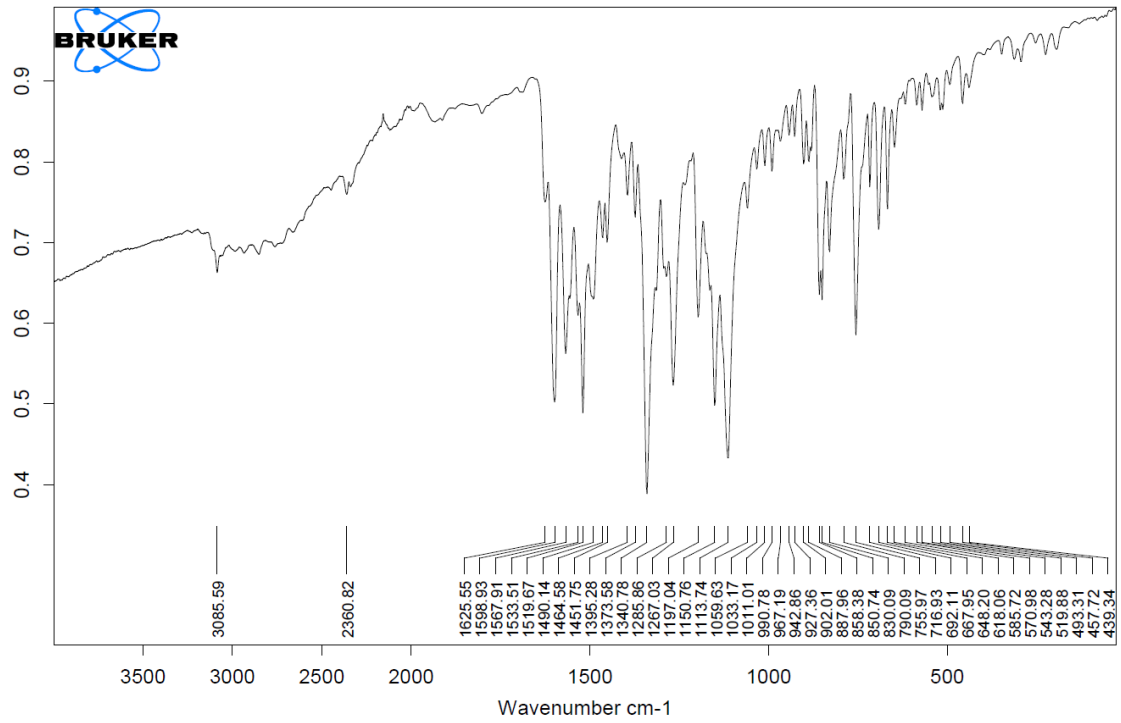

Figure S48. FT-IR spectrum of compound **3ea**.

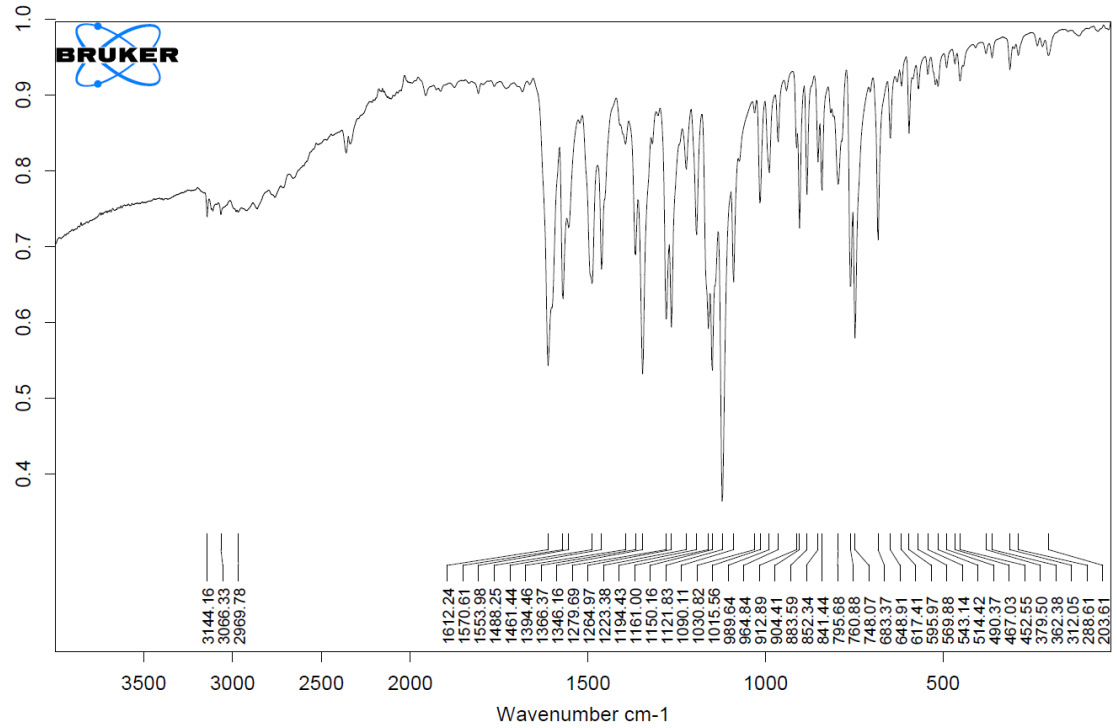

Figure S49. FT-IR spectrum of compound **3fa**.

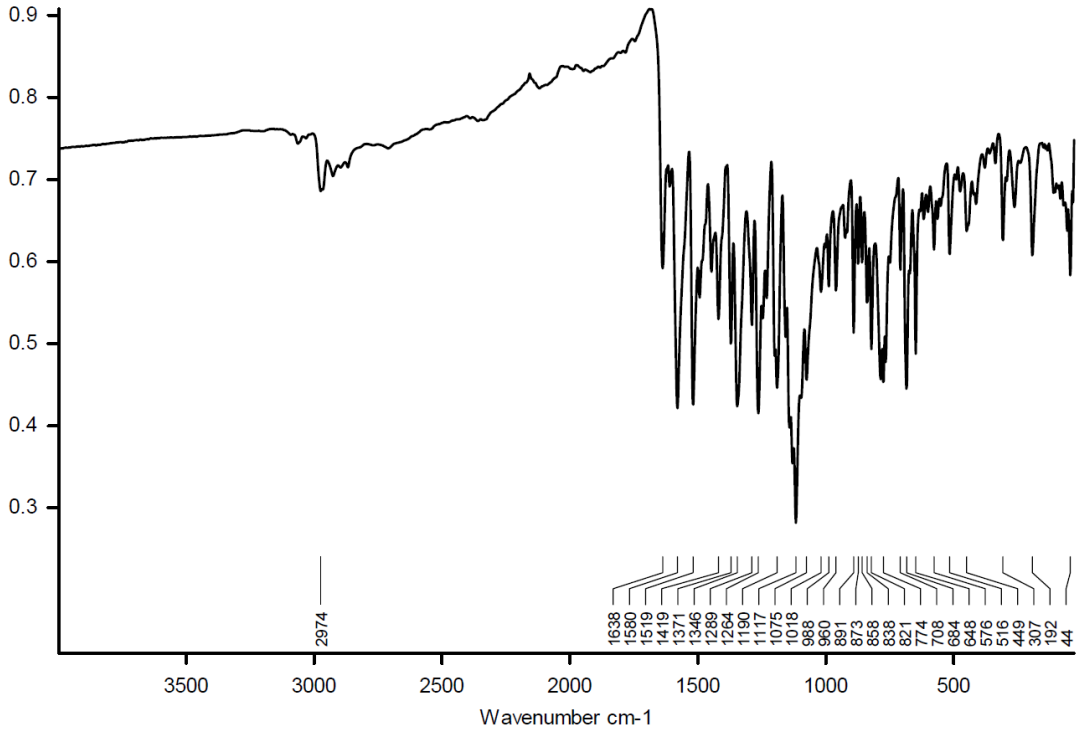

Figure S50. FT-IR spectrum of compound **3bb**.

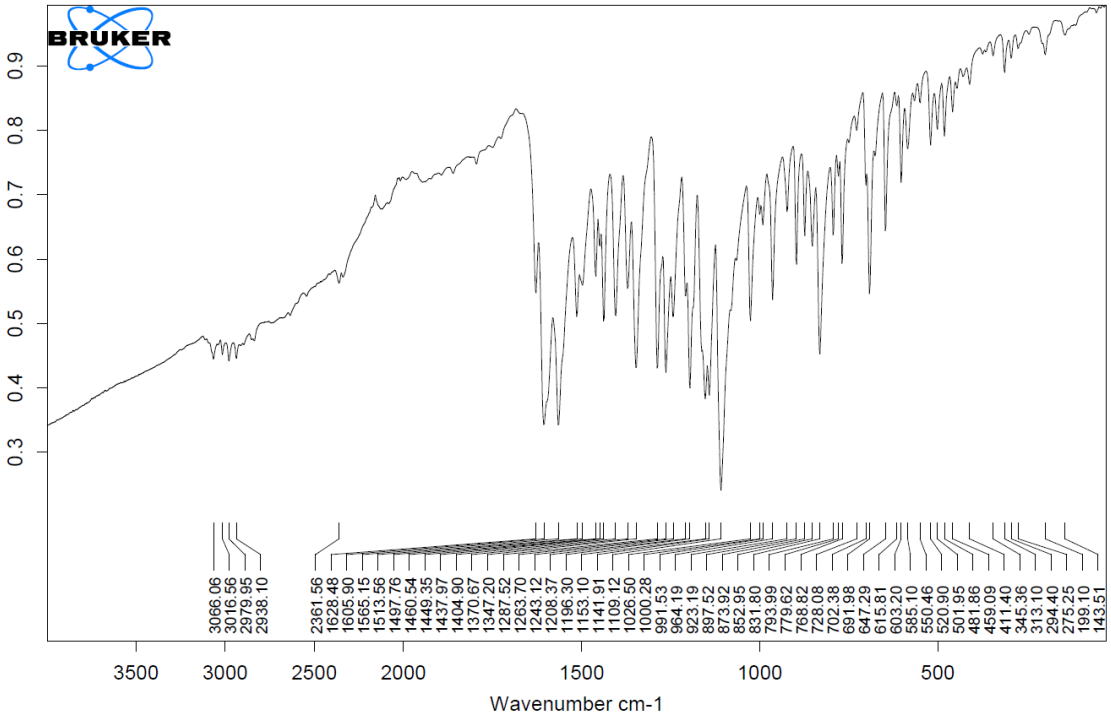

Figure S51. FT-IR spectrum of compound **3bc**.

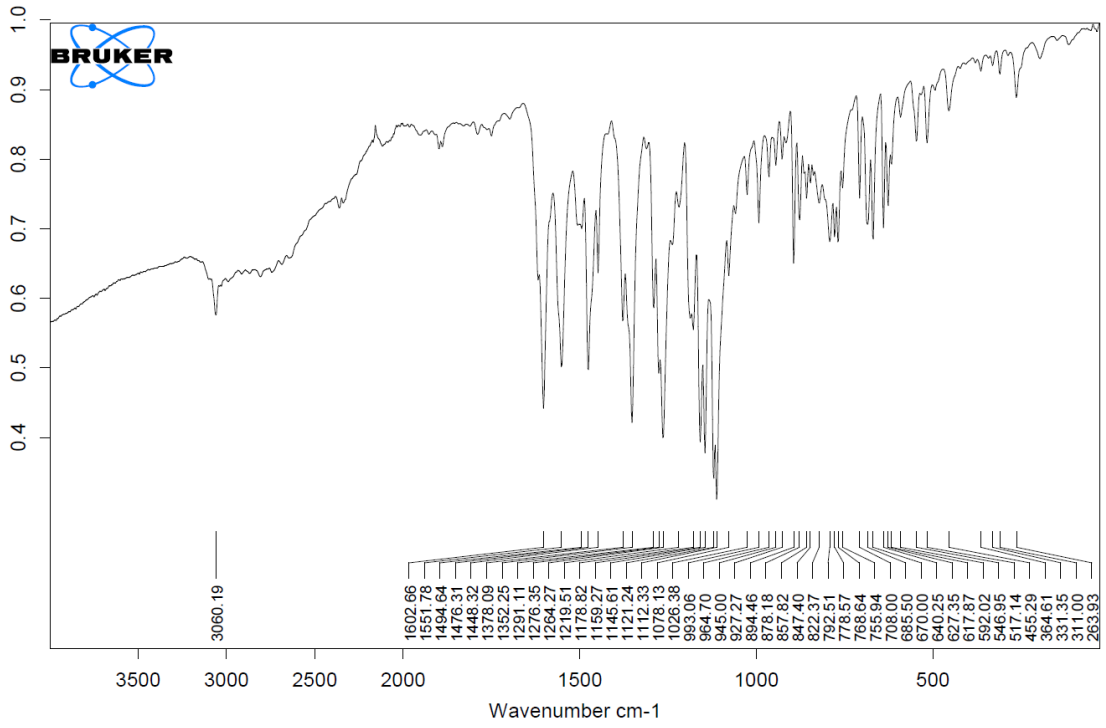

Figure S52. FT-IR spectrum of compound **3bd**.

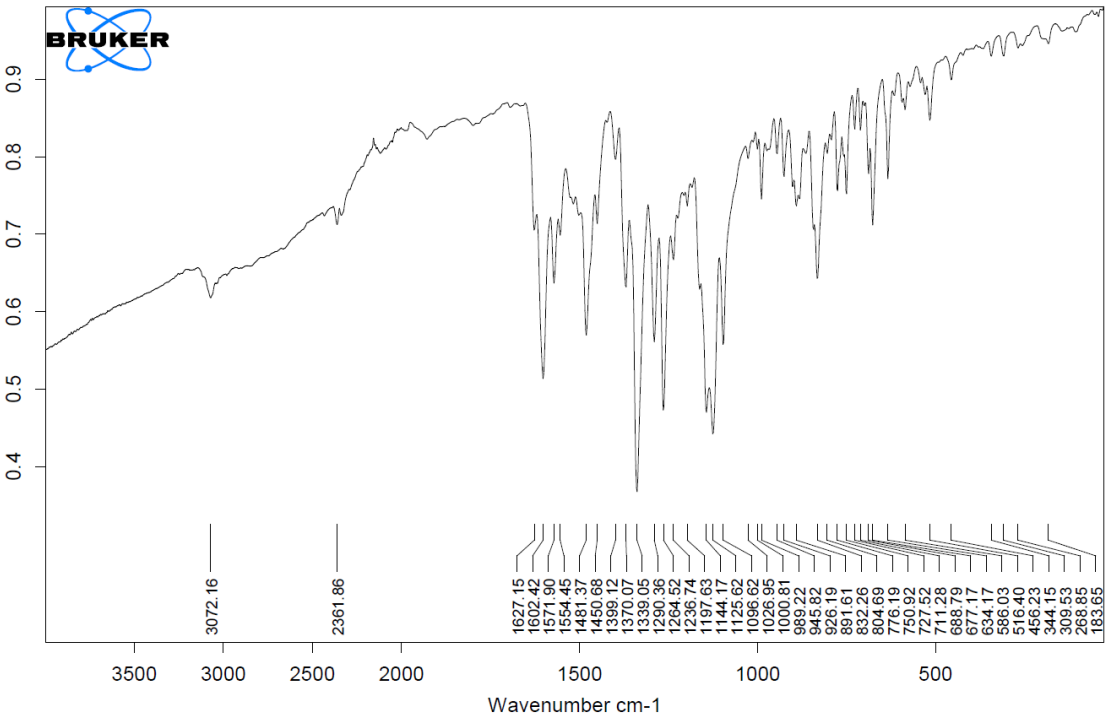

Figure S53. FT-IR spectrum of compound **3be**.

References

(1) Farrugia, L. J. *J. Appl. Crystallogr.* **2012**, *45* (4), 849–854. doi:10.1107/S0021889812029111

(2) Sheldrick, G. M. *Acta Crystallogr. Sect. A Found. Crystallogr.* **2008**, *64* (1), 112–122. doi:10.1107/S0108767307043930

(3) Basso, G.; Cargnelutti, J. F.; Oliveira, A. L.; Acunha, T. V.; Weiblen, R.; Flores, E. F.; Iglesias, B. A. *J. Porphyr. Phthalocyanines* **2019**, *23* (9), 1041–1046. doi:10.1142/S1088424619500767

(4) Guterres, K. B.; Rossi, G. G.; Menezes, L. B.; Anraku de Campos, M. M.; Iglesias, B. A. *Tuberculosis* **2019**, *117* (May), 45–51. doi:10.1016/j.tube.2019.06.001

(5) Silveira, C. H. da; Vieceli, V.; Clerici, D. J.; Santos, R. C. V.; Iglesias, B. A. *Photodiagnosis Photodyn. Ther.* **2020**, *31* (June), 101920. doi:10.1016/j.pdpdt.2020.101920

(6) Pivetta, R. C.; Auras, B. L.; Souza, B. de; Neves, A.; Nunes, F. S.; Cocca, L. H. Z.; Boni, L. De; Iglesias, B. A. *J. Photochem. Photobiol. A Chem.* **2017**, *332*, 306–315. doi:10.1016/j.jphotochem.2016.09.008

(7) Tanielian, C.; Golder, L.; Wolff, C. *J. Photochem.* **1984**, *25* (2–4), 117–125. doi:10.1016/0047-2670(84)87016-1